

The role of aqueous alteration in the formation of martian soils

Joshua L. Bandfield^{a,*}, A. Deanne Rogers^b, Christopher S. Edwards^c

^a Department of Earth and Space Sciences, University of Washington, Seattle, WA 98195-1310, United States

^b Department of Geosciences, Stony Brook University, 255 Earth and Space Sciences, Stony Brook, NY 11794-2100, United States

^c School of Earth and Space Exploration, Arizona State University, Tempe, AZ 85287-6305, United States

ARTICLE INFO

Article history:

Received 31 December 2009

Revised 25 August 2010

Accepted 27 August 2010

Available online 15 September 2010

Keywords:

Mars, Surface

Spectroscopy

Geological processes

Regoliths

Infrared observations

ABSTRACT

Martian equatorial dark regions are dominated by unweathered materials and it has often been assumed that they have not been significantly altered from their source lithology. The suite of minerals present is consistent with a basaltic composition and there has been no need to invoke additional processes to explain the origin of these compositions. We have begun to question this result based on detailed observations using a variety of datasets. Locally derived dark soils have a mineralogy distinct from that of adjacent rocky surfaces; most notably a lower olivine content. This pattern is common for many surfaces across the planet. Previous work using detailed measurements acquired within the Gusev Plains has shown that olivine dissolution via acidic weathering may explain chemical trends observed between rock rinds and interiors. Mineralogical trends obtained from rocks and soils within the Gusev Plains are more prominent than the elemental trends and support previous results that indicate that dissolution of olivine has occurred. However, clear differences are also present in elemental abundances that indicate a variety of inputs and processes are likely responsible for the formation of martian dark soils. Despite the potential complexity of source materials and processes, it appears that most martian dark regions have likely experienced aqueous alteration and chemical weathering appears to be closely linked to the mechanical breakdown of materials. Regardless of the responsible mechanism, there appears to be a general, though not perfect, correlation between elevated olivine abundance and high-thermal inertia surfaces on Mars.

© 2010 Elsevier Inc. All rights reserved.

1. Introduction

A major goal of martian exploration is to understand how much and under what conditions liquid water has been present throughout martian history. This record of aqueous processes can be revealed from characteristics such as elemental composition and mineralogy, landscape morphology, stratigraphic relationships, and surface textures. Over the past decades, spacecraft have returned data that have enabled construction of at least a rudimentary global understanding of aqueous processes on Mars using these characteristics.

Elemental composition and mineralogy can give a positive indication of the presence of liquid water at the time of formation. Although not without ambiguity, elemental and spectroscopic observations of Mars have provided a wealth of evidence for aqueous processes. These observations have provided positive evidence for chemical sedimentary compositions such as sulfates (e.g. Gendrin et al., 2005) or weathering products such as certain types of phyllosilicates (e.g. Poulet et al., 2005). Concentrations of elements such as sulfur or chlorine also indicate the presence of water

that would concentrate elements that are typically found in more soluble species (e.g. Clark, 1981; Keller et al., 2006; Gellert et al., 2006). Other elemental and mineralogical trends are also indicative of chemical alteration under specific conditions (e.g. Hurowitz et al., 2006) and both orbital and in situ observations have provided an increasingly detailed picture of properties such as the temperature, pH, and abundance of water present.

Despite this evidence for aqueous processes at many locations, martian equatorial dark regions (largely coincident with Surface Type 1 of Bandfield et al. (2000)) have been interpreted as unweathered materials that have not been significantly altered from the source material (e.g. Bandfield et al., 2000; Mustard et al., 2005). Spectroscopic observations from visible through thermal infrared (TIR) wavelengths indicate the presence of plagioclase, pyroxene, and minor amounts of olivine (e.g. Rogers and Christensen, 2007) throughout low latitude low albedo martian surfaces. This suite of minerals is consistent with a basaltic composition and, given this information, there was no apparent need to invoke additional processes to explain the presence of these materials on the martian surface.

We and others have begun to question this assumption based on detailed observations from a variety of datasets (McSween et al., 2006; Bandfield and Rogers, 2008; Amundson et al., 2008; Rogers et al., 2009). The work that we present here integrates a

* Corresponding author.

E-mail address: joshband@u.washington.edu (J.L. Bandfield).

variety of local and global observations that indicate a link between source rocks and dark soils (the term “soil” as it is used here refers to the finer fraction of the martian regolith and does not imply organic content) on Mars. Relatively low thermal inertia dark soils have a distinctive mineralogy from that of local and regional high-thermal inertia rocks and rocky surfaces. Investigation of elemental and mineralogical relationships between rocks and soils appears to indicate that aqueous alteration is an important process in the formation of martian dark soils.

On Earth, rocky surfaces are typically broken down into finer sediments through a combination of chemical and physical weathering and soils are typically composed of both primary and secondary compositions (e.g. Jenny, 1941). Although similar processes may be present on Mars, soil formation mechanisms remain poorly understood. There are a number of basic questions that remain largely unanswered when considering soil formation mechanisms on Mars: What are the relative roles of chemical and mechanical weathering in martian soil formation? How do processes such as meteor impacts or aeolian erosion of friable materials contribute to soil formation? Most martian low albedo regions have properties consistent with silty and sandy soils (e.g. Kieffer et al., 1977) and there are basic and fundamental outstanding questions about the formation and development of these surfaces that cover a substantial portion of Mars.

2. Data and methods

2.1. Themis

For this work, we used 2001 Mars Odyssey Thermal Emission Imaging System (THEMIS) nighttime temperature data for the derivation of surface thermophysical properties and daytime multispectral data was used to derive surface compositional information. THEMIS has a thermal imaging subsystem that consists of a 320 by 240 pixel uncooled microbolometer array. Multispectral images are acquired in a pushbroom fashion using filters in nine spectral bandpasses between ~ 7 and $15 \mu\text{m}$. Spatial sampling is ~ 100 m from a ~ 400 km near-circular orbit. Detailed descriptions of radiometric uncertainties and calibration methods are described in Christensen et al. (2004), Bandfield et al. (2004a), and Fergason et al. (2006a).

2.2. THEMIS derived thermal inertia

We used thermal inertia derived from THEMIS nighttime temperature data to identify surfaces dominated by rocks and surfaces consistent with soil cover. The KRC thermal model (H.H. Kieffer, manuscript in preparation) was used for this work to predict surface temperatures for a given set of thermophysical properties. This model has been used in many studies for a variety of applications (e.g. Titus et al., 2003; Kieffer et al., 2006; Fergason et al., 2006a,b; Bandfield and Feldman, 2008; Bandfield and Edwards, 2008). In the application as used here, a single pre-dawn temperature is converted to a thermal inertia value using a temperature to inertia lookup table produced using the local conditions for each site (e.g. latitude, albedo, L_s).

We used the results of Edwards et al. (2009) to identify the global occurrences of rock dominated surfaces. In that study, thermal inertia values were derived from the maximum pixel temperature in each ~ 32 by 26 km segment of nighttime THEMIS images. A thermal inertia value of $>1200 \text{ J m}^{-2} \text{ K}^{-1} \text{ s}^{-1/2}$ (these units are used throughout this manuscript to describe thermal inertia values) was defined as indicative of a surface dominated by rocky materials and each occurrence was documented along with the associated morphological characteristics. The high inertia surfaces could be cate-

gorized as one of three surface types; (1) steep surfaces of crater and canyon walls; (2) crater floors; and (3) inter-crater plains surfaces. Rocky surfaces were found by Edwards et al. (2009) to be uncommon on Mars, covering much less than 1% of the surface.

We use the crater floor and inter-crater plains high-thermal inertia surfaces for comparison with global compositional data. Although steep surfaces are the most common occurrence of high inertia surfaces, their high slope angles, relatively small exposures, and often spur and gully morphology make compositional investigations extremely difficult. For this reason, we have not included these steep surfaces in the work presented here.

In addition to global high inertia identifications, thermal inertia was derived on a per-pixel basis from individual THEMIS nighttime temperature images. We used a methodology similar to that of Fergason et al. (2006a) and uncertainties are described in detail in that work. Although parameters such as surface slope and albedo were not incorporated in the thermal modeling at the spatial resolution of the temperature measurements, the pre-dawn temperatures have a relatively low sensitivity to these parameters. The methodology used here is well suited for the purpose of distinguishing dusty, sandy/silty, and rocky surfaces (Fergason et al., 2006a). The high resolution thermal inertia data was used for comparison with spatially coincident compositional information (described below).

2.3. THEMIS compositions

Daytime multispectral THEMIS data were used to assess the composition of the surface. Although the limited spectral information prevents retrieval of detailed mineralogical information, spectral units can be linked to lower spatial resolution but higher spectral resolution Thermal Emission Spectrometer (TES) data. This type of analysis leverages the capabilities of both datasets and has been effectively used in previous work (e.g. Bandfield et al., 2004a; Rogers et al., 2005; Schnieder and Hamilton, 2006; Rogers and Bandfield, 2009).

Olivine-rich surfaces are readily identified in decorrelation stretch (DCS; Gillespie et al., 1986) images using daytime THEMIS radiance data (e.g. Hamilton and Christensen, 2005; Rogers et al., 2005). These images have allowed for a rapid assessment of spectral components within several thousand THEMIS images, providing a global assessment of olivine-rich surfaces. The analysis is necessarily qualitative and subject to both errors of omission and commission. In addition, any global assessment is subject to data coverage, which is relatively sparse for warm (average temperature >240 K) daytime data in the northern hemisphere. However, more detailed analyses (described below) have been used to perform checks on these olivine-rich surface identifications, ensuring that the overall geographical trends are accurate and errors of commission are not common.

It is necessary to account for atmospheric effects properly in order to retrieve quantitative spectral information. THEMIS data were corrected using the methods described in detail in Bandfield et al. (2004a). In this method, atmospheric emission and secondary scattering are calculated directly from the THEMIS data using a region of assumed constant emissivity, but variable surface temperature. Atmospheric attenuation is then determined by defining surface emissivity for a large area within a THEMIS image from lower resolution TES data. The same atmospheric properties can be then be applied to correct each THEMIS pixel at its full spatial resolution.

Linear deconvolution (e.g. Ramsey and Christensen, 1998) is used to determine the concentrations and distributions of spectral components within the THEMIS images. In this application, spectral endmembers were selected both from the image itself and from external sources such as surface dust derived from TES data

(Bandfield and Smith, 2003) or laboratory emissivity data of olivine. The limited spectral information in the THEMIS data only allows for the mapping of a few spectral units and it is often difficult to retrieve detailed mineralogy. However, the spectral signature of olivine at TIR wavelengths is distinct and can be cleanly separated from other spectral components in the THEMIS data (Rogers and Bandfield, 2009).

Thermal inertia and compositional data were derived from coincident surfaces using overlapping daytime and nighttime data. This allows for quantitative comparisons of these two parameters to assess the relationship between compositional units and the general particle size distributions present. There are spatial uncertainties of several hundred meters in the projected daytime and nighttime THEMIS data and the comparison of datasets requires visual co-registration. These uncertainties will lead to minor amounts of misregistered data near unit boundaries. However, general correlations can be easily identified and distinguished, especially because the spatial extent of spectral and thermophysical units is much larger than the spatial registration uncertainty.

2.4. HiRISE/CRISM

Surface morphology and textures are often correlated with thermophysical and compositional units (e.g. Edwards et al., 2009; Rogers et al., 2009). In particular, high-thermal inertia surfaces often appear highly fractured in sub-meter sampling images and are often lighter toned than surrounding dark soils. It can be somewhat difficult to correlate sub-meter textures identified in High Resolution Imaging Science Experiment (HiRISE; McEwen et al., 2007) images with the 100 m/pixel THEMIS data because of the large difference in spatial resolution.

We used ~18 m/pixel Compact Reconnaissance Imaging Spectrometer for Mars (CRISM; Murchie et al., 2007) data to serve an intermediate resolution spectral imaging dataset that could bridge the spatial resolution gap between the THEMIS and HiRISE datasets. CRISM has a spectral range of 0.36–3.92 μm with a sampling of 0.066 $\mu\text{m}/\text{channel}$ and full resolution target (FRT) data covers an area of $\sim 12 \times 12$ km. Full and half resolution data are acquired using the single axis pointing capability of the optical sensor unit that allows for ground motion compensation and acquisition of emission phase function measurements. Murchie et al. (2007) provides a detailed description of the CRISM instrument characteristics and investigation.

Although it is difficult to retrieve quantitative mineralogical abundance information from near- and short wave infrared (NIR and SWIR) spectral reflectance measurements, it is possible to map the intensity of characteristic mineral absorptions, which may be a qualitative indicator of abundance. We use spectral indices similar to those described by Pelkey et al. (2007) to show the distribution of olivine-rich and other materials in CRISM FRT data (e.g. Mustard et al., 2009). Data were corrected for atmospheric gas absorptions using the “volcano scan” technique that utilizes observations over a relatively uniform surface with variable elevation to isolate atmospheric absorptions (Pelkey et al., 2007; McGuire et al., 2009). The CRISM data were not corrected for atmospheric aerosols that can interfere with the intensity of broad absorptions such as those of olivine, especially with the variable viewing geometry of CRISM targeted images.

Visual comparisons of CRISM olivine index images with THEMIS olivine concentration images show that, for the regions examined in this work, the NIR and TIR datasets are highly correlated and that alteration, coatings, particle size effects, or other environmental parameters do not cause any apparent mismatch between the two datasets. This correlation makes CRISM data well suited to link the spatial resolution gap between THEMIS olivine concentration data and HiRISE images.

2.5. Mini-TES

Bulk mineralogy of rocks and dark soils within the Gusev Plains was derived from Miniature Thermal Emission Spectrometer (Mini-TES; Christensen et al., 2003) data. Mini-TES is a Fourier Transform Michelson Interferometer with a spectral range of 340–2000 cm^{-1} ($\sim 29\text{--}5$ μm) and 10 cm^{-1} sampling. Mini-TES has a Cassegrain telescope that views out of the ~ 1.5 m tall Pancam Mast Assembly (PMA) with field of view of 20 mrad, resulting in a measurement spot size of 0.2 m from a distance of 10 m. Target measurements typically include averaging of 5–100 successive spectra to increase the signal to noise ratio. Christensen et al. (2003) provides a detailed description of the Mini-TES instrument characteristics and investigation.

A number of corrections for atmospheric and dust radiance sources are applied to the Mini-TES data, which are described in detail in Ruff et al. (2006). Briefly, downwelling atmospheric radiance reflected off the target surface is corrected assuming a simple relationship between reflectance and emissivity ($R = 1 - \epsilon$) and using a sky observation acquired within a short time before or after the target measurement. After sol 420 at Gusev Crater, an additional correction is required to compensate for a dust coating on the PMA mirror. This correction was applied in a similar manner as that described by Ruff et al. (2006) with a modification that treats the dust as an isothermal opacity layer between the instrument and target. This layer is assumed to be at the temperature of the mirror assembly. Finally, an additional correction is necessary to compensate for a poorly understood dust radiance contribution. Although the spectral character of this correction is well known and the effect appears to be linear, the magnitude of the correction is variable. The magnitude can be obtained by including an atmospheric dust spectral shape as a spectral endmember in deconvolution (Ruff et al., 2006).

Corrected emissivity spectra are analyzed based on a qualitative visual inspection of absorption features and spectral endmember deconvolution. Simple visual inspection can be used to identify the presence of phases such as olivine that have prominent and relatively narrow absorptions. However, the surface materials on Mars are often composed of multiple phases, which mix in an approximately linear fashion in thermal infrared data (e.g. Tompson and Salisbury, 1993; Ramsey and Christensen, 1998). Absorptions from mixtures of materials, such as silicates, sulfates, and oxides often have broad absorptions with subdued spectral features.

Deconvolution analysis has been applied to laboratory and remotely sensed data of Earth and Mars in numerous studies, including several using Mini-TES data (e.g. Ramsey and Christensen, 1998; Hamilton and Christensen, 2000; Bandfield et al., 2000; Bandfield et al., 2004b; Glotch et al., 2006; Rogers and Aharonson, 2008; Ruff et al., 2006). The specific method applied here is the method of Rogers and Aharonson (2008) that restricts the least-squares fit of the measured spectra to use only positive endmember concentrations. The iterative method of Ramsey and Christensen (1998) converged on a local minimum by rejecting endmembers with negative concentrations using repeated unrestricted linear least-squares fits. The method of Rogers and Aharonson (2008) uses a method to converge on the global minimum least-squares fit of the measured spectrum while retaining the non-negative constraint, resulting in a more accurate model.

Uncertainties in the deconvolution model are reported for each model fit of the measured spectra and depend on characteristics such as spectral absorption depths and contrast with other endmember spectra. These uncertainties are typically near 5–10% abundance. A larger source of uncertainty is due to systematic effects that can result from incorrect removal of radiance components and systematic bias in the calibration of the data. These

uncertainties are more difficult to characterize, but have typically been addressed by utilizing multiple independent measurements, data correction techniques, or applied under variable conditions (e.g. Smith et al., 2000; Bandfield et al., 2004a; Rogers and Aharonson, 2008).

2.6. APXS

Alpha Proton X-ray Spectrometer (APXS) derived oxide abundances were used to compare the elemental composition of various materials in the Gusev Plains. The APXS exposes the measurement surface with alpha particles and X-rays. Elemental abundances are derived from the measurement of the energy distribution of back-scattered alpha particles and X-rays (Rieder et al., 2003). We use the APXS derived oxide abundances archived at the Planetary Data System and processed using the fit program, method, and calibration parameters described in Gellert et al. (2006). Measurements used in this study include Adirondack Class rocks as well as dark soils. A detailed description of the APXS instrument, measurements, and calibration is found in Rieder et al. (2003) and Gellert et al. (2006).

3. Results

3.1. Global bedrock and olivine unit distributions

Fig. 1 shows the global distribution of high-thermal inertia (>1200) surfaces and olivine-rich surfaces identified in THEMIS decorrelation stretch images. Both distributions show a strong dependence on both albedo and latitude. Almost all olivine-rich and high inertia surfaces are located within $\pm 45^\circ$ latitude. With several exceptions, both types of surfaces are also located within low albedo regions and are not typically found within moderate to high albedo dusty regions such as Arabia, Tharsis, and Elysium. Although the regional association is strong, olivine-rich and high-thermal inertia exposures are not necessarily coincident. For example, both Ares Valles and the southern rim of Isidis Basin have extensive exposures of olivine-rich surfaces, but lack surfaces with thermal inertia values that exceed 1200.

There are extensive low latitude, low albedo regions that do not contain any exposures of either high-thermal inertia or olivine-rich surfaces. For example both Tyrrhena Terra and Meridiani Planum are equatorial low albedo regions that do not have these surface

types. The global distribution of the olivine-rich high-thermal inertia surfaces appears to form regional clusters independent of their association with latitude and albedo.

3.2. Regional examples: Isidis Planitia and Nili Fossae

3.2.1. Comparisons of thermal inertia and olivine abundance

Nili Fossae and the southern rim of Isidis Basin were selected for more detailed analyses. Regional mosaics of both regions are shown in Figs. 2 and 3. A qualitative comparison of nighttime temperature data and DCS images shows a high degree of spatial correlation between olivine-rich surfaces and high-thermal inertia surfaces. This is based on the interpretation of relatively warm nighttime surfaces as having a higher thermal inertia than lower nighttime temperature surfaces. A qualitative compositional interpretation of olivine-rich surfaces is based on purple and magenta colors in band 8–7–5 (projected as red–green–blue) DCS images.

In the case of the southern rim of Isidis Basin, the olivine-rich, high-thermal inertia surfaces are concentrated within the plains immediately adjacent to the mountainous terrain to the south. Exposures are present in small isolated areas further within Isidis Basin, often in association with craters. The spatial distribution of olivine-rich and high-thermal inertia surfaces is more complex in the case of Nili Fossae. Although the two surface types are also highly correlated, important exceptions also exist. There are surfaces that appear lavender in color in the decorrelation stretch mosaic of Nili Fossae that correspond to relatively cool nighttime temperatures. This indicates that relatively low thermal inertia olivine-rich surfaces are present in this region. In addition, there are surfaces with relatively warm nighttime temperatures that appear as indistinct shades of green in the decorrelation stretch mosaic, indicating that there are olivine-poor surfaces may have high-thermal inertia. Because atmospheric and surface temperature conditions vary between individual THEMIS images, colors vary within the mosaics, making quantitative comparisons of data difficult in this format. The results presented here are similar to observations in Nili Fossae made by Hamilton and Christensen (2005) and in the southern rim of Isidis Basin made by Tornabene et al. (2008).

Thermal inertia values were derived from a single nighttime THEMIS image within each of the regions covered by the mosaics (Fig. 4). Because the derivation only used a one dimensional lookup table to convert surface temperature to thermal inertia (using the

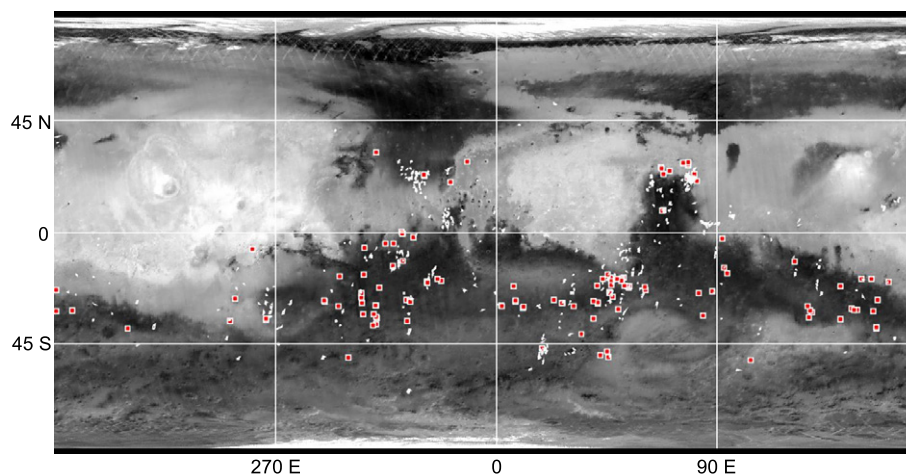


Fig. 1. Plains and crater floor high inertia surfaces (red squares) of Edwards et al. (2009) and olivine-rich surfaces identified in THEMIS DCS images (white outlines). The background image is TES derived albedo. Both types of surfaces are typically associated with low latitude and low albedo surfaces. Several equatorial low albedo regions do not contain either high-thermal inertia or olivine-rich surfaces. (For interpretation of the references to color in this figure legend, the reader is referred to the web version of this article.)

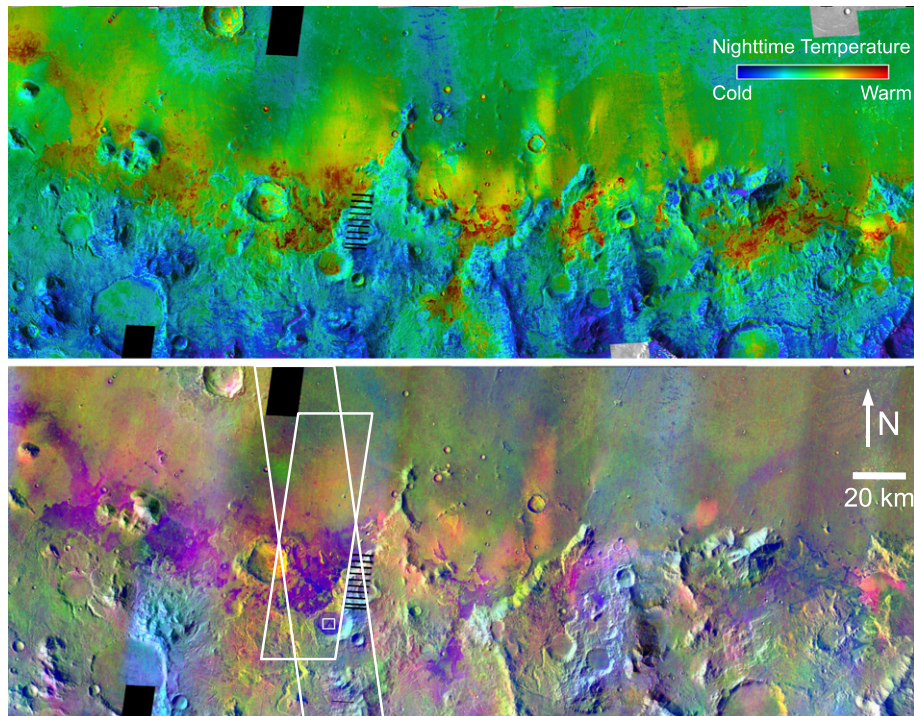


Fig. 2. THEMIS image mosaics covering the southern rim of Isidis Basin. The top image shows THEMIS nighttime band 9 radiance in color with daytime band 9 radiance as shading. Warmer night time temperatures are interpreted to be relatively high-thermal inertia surfaces. The bottom image shows daytime THEMIS DCS radiance data using bands 8–7–5 projected as red, green, and blue respectively. Olivine-rich surfaces are interpreted to be shades of purple and magenta. The mosaics are centered near 86E, 4N. The boxes denote the areas covered by thermal inertia data (larger box), concentration maps (smaller box), and detail images (tiny box) shown in Figs. 4, 5 and 9 respectively. (For interpretation of the references to color in this figure legend, the reader is referred to the web version of this article.)

same input parameters for all surfaces), the resulting thermal inertia image is qualitatively similar to the nighttime surface temperature image. The image covering the southern rim of Isidis Basin displays low inertia values of ~ 100 – 200 in the rugged terrain to the south, ~ 400 – 600 in the immediately adjacent plains and ~ 200 – 300 towards the north. Thermal inertia values cover a similar range in the Nili Fossae example, except the high-thermal inertia surfaces have somewhat lower values (~ 300 – 500) and lower inertia surfaces have values of ~ 150 – 300 . The spatial pattern of the surfaces is complex though, as can also be seen in the nighttime temperature mosaic, surfaces within topographic lows often have low thermal inertia values.

Deconvolution using spectral endmembers was applied to a daytime THEMIS image over a region coincident with the derived thermal inertia values. In the case of the southern rim of Isidis Basin, three spectral endmembers were used (Fig. 5); an image endmember similar to the Surface Type 1 of Bandfield et al. (2000); surface dust derived from TES emission phase function measurements (Bandfield and Smith, 2003) convolved with the THEMIS spectral bandpasses; and olivine-rich basalt derived from TES measurements. Average root mean square (RMS) errors are 0.0011 and all pixels were fit with RMS errors of < 0.0073 in emissivity. The THEMIS data is well modeled and there is no need to include other spectral components to accurately model the data.

Deconvolution results are similar for a THEMIS image within Nili Fossae (Fig. 6). Three spectral endmembers were used; in this case a high silica component similar to the Surface Type 2 of Bandfield et al. (2000) was used and the surface dust component was not included. The spatial distribution of the spectral endmembers is complex, similar to the thermal inertia distributions. Average RMS errors for this image are 0.0013 with a maximum of 0.0112. Higher errors are typically associated with colder surfaces that have higher noise.

It is possible to quantitatively compare the thermal inertia and deconvolution results where they cover the coincident surfaces. Fig. 7 shows the thermal inertia distributions of pixels that have a concentration of 0.9 or greater of one of the spectral endmembers. This method shows the distributions more clearly without significant mixing of surface compositional types. In the case of the southern rim of Isidis Basin, the dust, basaltic, and olivine-rich endmembers have thermal inertia distributions that are cleanly separated. This separation is not as clear in the case of Nili Fossae. The Surface Types 1 (basaltic) and 2 (silica-rich) spectral endmembers have similar thermal inertia values, though the Surface Type 2 has a narrower distribution of thermal inertias. As with the southern rim of Isidis, the olivine-rich surfaces have higher thermal inertia values than the surrounding terrain. However, there is a lower thermal inertia tail in the Nili Fossae olivine-rich surface distribution that shows clear overlap with the other surface types.

3.2.2. Comparisons of morphology and olivine abundance

Several locations were selected for a more detailed comparison of olivine-rich surfaces and surface texture and morphology in high-resolution images. We chose isolated locations within the southern rim of Isidis Basin and Nili Fossae in the regions discussed above. In addition high-resolution images have been acquired in Ares Valles and Argyre Planitia, which have been the focus of previous studies (Rogers et al., 2005; Buszkowski et al., 2008; Bandfield and Rogers, 2008).

Locations within Nili Fossae and the southern rim of Isidis that have high resolution HiRISE and CRISM coverage were selected. The first image is located within Nili Fossae (Fig. 8). The CRISM olivine index displays olivine absorptions that are clearly correlated with the lower spatial resolution THEMIS data. Aeolian ripples are present throughout the olivine-rich terrain. However, olivine absorptions are subdued where the ripples dominate the

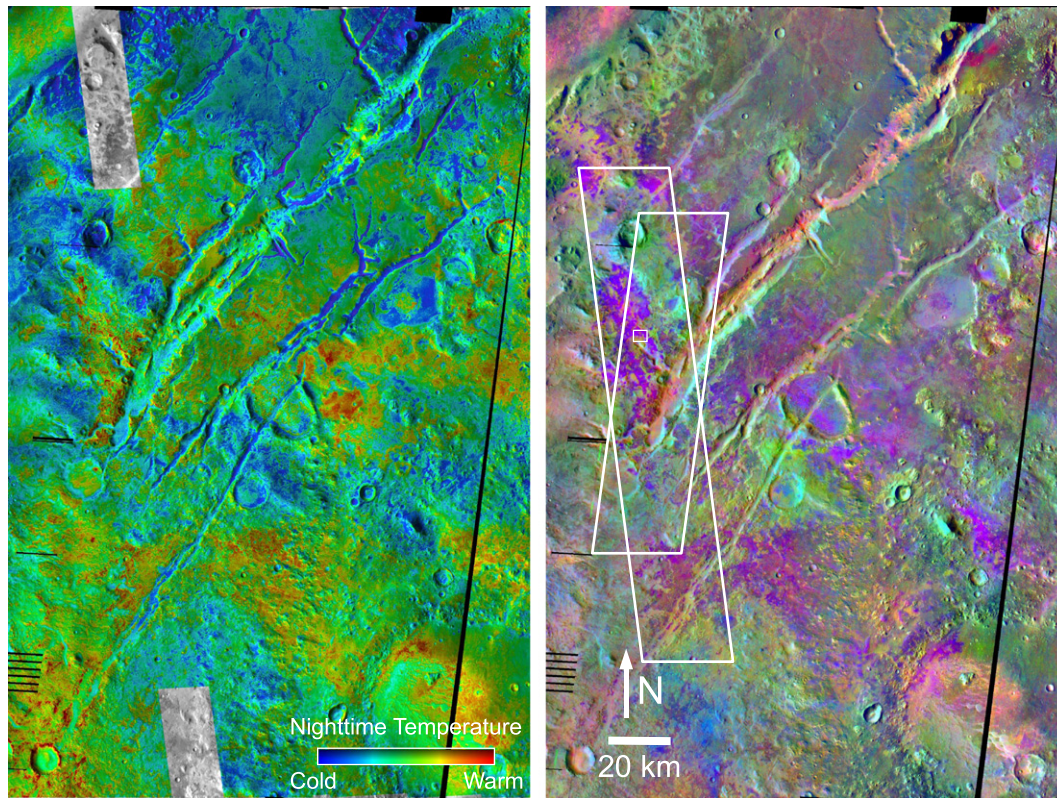


Fig. 3. THEMIS image mosaics covering a portion of Nili Fossae. The left image shows THEMIS nighttime band 9 radiance in color with daytime band 9 radiance as shading. Warmer night time temperatures are interpreted to be relatively high-thermal inertia surfaces. The bottom image shows daytime THEMIS DCS radiance data using bands 8–7–5 projected as red, green, and blue respectively. Olivine-rich surfaces are interpreted to be shades of purple and magenta. The mosaics are centered near 78E, 22N. The boxes denote the areas covered by thermal inertia data (larger box), concentration maps (smaller box), and detail images (tiny box) shown in Figs. 4, 6 and 8 respectively. (For interpretation of the references to color in this figure legend, the reader is referred to the web version of this article.)

surface and they are generally present where the terrain appears to be highly fractured (Figs. 8 and 9). In some areas, strong olivine absorptions are associated with smooth featureless areas in HiRISE images. These regions have high-thermal inertia values consistent with rocky surfaces. Low thermal inertia, less fractured ripple-free surfaces are present in the area, but they do not contain olivine-rich compositions.

The second image within the southern rim of Isidis Basin is located within what appears to be a filled-in crater within the mountainous terrain to the south (Mustard et al., 2009; Fig. 10). The CRISM olivine index is consistent with the THEMIS compositional data. The aeolian ripples are again present as before and can be seen in high-resolution images, but the underlying terrain is often layered without the pervasive fracturing that is present on the olivine-rich surfaces to the north.

3.3. Local example: Gusev Plains

Observations and measurements in the Gusev Plains were limited to dark soils and Adirondack Class rocks. One exception is the use of El Dorado sand measurements because they may be similar in origin and composition to other dark dune forms observed from orbit. Brighter soils presumably have a global dust contribution that is not necessarily locally derived. Soils and rocks within the Columbia Hills were also excluded because they appear to have a considerably more complex relationship to one another and are not representative of martian dark plains. Indeed, orbital spectroscopic datasets have not detected the diversity indicated by the MER measurements in the Columbia Hills.

Table 1 shows a list of APXS and Mini-TES observations used in this study. Mini-TES observations were grouped into dark soils,

clean rock surfaces, or dune surfaces. The dark soil surface spectra were retrieved from rover tracks, which largely removed the effects of bright dust and were warm enough to minimize environmental effects, such as reflected downwelling atmospheric radiance. The dark soil spectra are shown in Fig. 11. Although there are variations in spectral contrast, the basic spectral shapes are relatively constant. More variation is apparent in the rock spectra (Fig. 12), but all spectra have prominent absorptions near 390, 500, and 900 cm^{-1} that are not as prevalent in the dark soil spectra. Although the variation present in the rock spectra may be due to variations in composition, the rock spectra will also display variability due to the correction for dust contributions. The average rock-spectrum has absorption features consistent with the presence of olivine present near 500 and 900 cm^{-1} . The average El Dorado sand spectrum is shown in Fig. 13 along with the average soil and rock spectra. The El Dorado spectra have a spectral shape that is in-between that of the dark soils and rocks with the exception of minor differences in the shape and position of the longer wavelength (lower wavenumber) features.

APXS measurements were separated into three categories; dark soils, brushed rocks, and RATED rocks (Tables 2 and 3). Dark soils include trenches as well as rover track surfaces. The trenches were not included in the Mini-TES observations because they were typically too cold to provide adequate signal to noise ratios. The most notable difference between the average rock and dark soil compositions is an association of higher sulfur abundances with rock surfaces and especially dark soils as opposed to rock interiors. Most major cations (Mg, Al, Ca, Fe) show a decrease in abundance for rock surfaces and soils and Si content remains relatively constant. The El Dorado sand measurements are relatively unique in that they have relatively high Si, Mg, Al and relatively low S, Ca, and

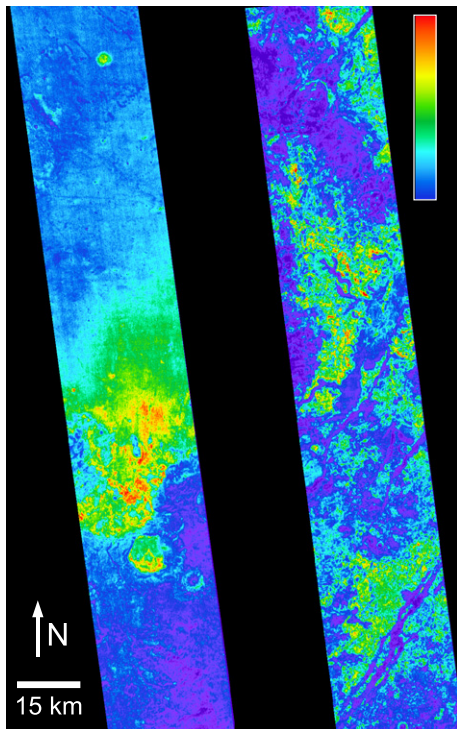


Fig. 4. Thermal inertia derived from THEMIS nighttime band 9 radiance data. The left image covers a portion of Isidis Basin shown in Fig. 2 (THEMIS ID I19050003). The right image covers a portion of Nili Fossae shown in Fig. 3 (THEMIS ID I01327002). The color scale represents a range of 200–600 and 150–500 $\text{J m}^{-2} \text{K}^{-1} \text{s}^{-1/2}$ for the left and right images respectively. (For interpretation of the references to color in this figure legend, the reader is referred to the web version of this article.)

Fe abundances. Minor element abundances show a correlation between Ti, Cl, K, Zn, and Ni, which are higher in the soils and rock surfaces than rock interiors.

3.3.1. Comparison of Gusev Plains spectra to orbital data

Average rock and soil Mini-TES spectra are shown with average equatorial dark surface and olivine-rich surface spectra derived from TES data (Fig. 13). The rocks in the Gusev Plains could not be directly detected by TES or THEMIS observations and the dark soils also have a thin dust covering. However, a comparison can be made to spectra of other equatorial dark soils and olivine-rich regions (Fig. 13). Similar to Yen et al. (2005), the low albedo surface spectrum of Bandfield and Smith (2003) was used for comparison to the Mini-TES dark soil spectrum. This was derived from multiple emission angle measurements from equatorial low albedo regions. Rogers et al. (2007) have shown that there are regional variations in the spectral character of equatorial low albedo regions, but they are generally subtle compared to differences present between low albedo soils and olivine-rich surfaces.

Olivine-rich surface spectra derived from TES data were obtained using the technique described in Bandfield (2008), which is not reliant on deconvolution or spectral libraries and has an extended wavelength range compared to the deconvolution atmospheric correction method (Smith et al., 2000). This method uses the gas removal techniques as well as the atmospheric dust opacity shape of Bandfield and Smith (2003) with knowledge of the $\sim 1100 \text{ cm}^{-1}$ emissivity of a nearby dusty surface to determine and remove the radiative contributions of atmospheric dust. Olivine-rich surfaces in Nili Fossae were used for comparison to Mini-TES data of Gusev Plains rocks. Narrow features are similar between both the Nili Fossae and Gusev surfaces although the fea-

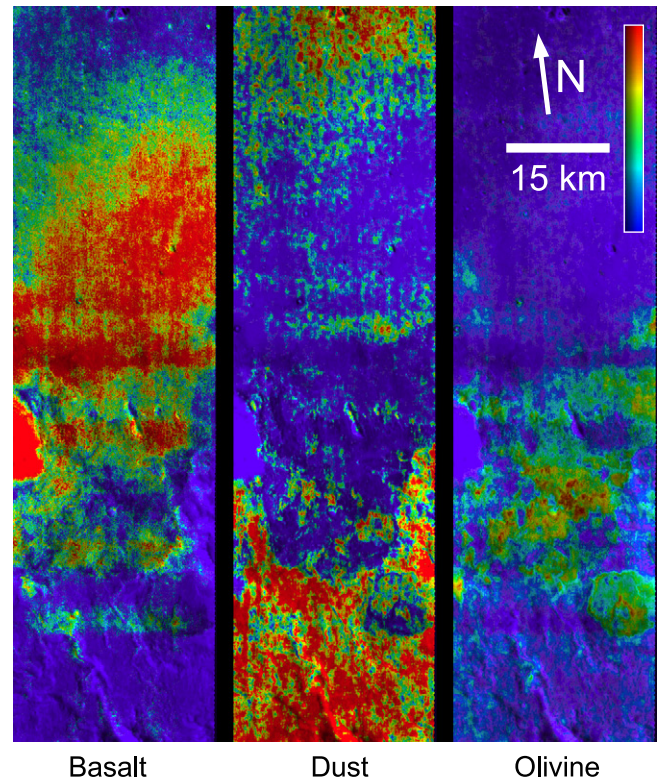


Fig. 5. Isidis Basin spectral endmember concentration maps for the region shown in Fig. 2 (THEMIS ID I01395005). The left image (basalt) shows concentrations of materials dominated by plagioclase and pyroxene, the center image (dust) shows concentrations of dusty surfaces, and the right image (olivine) shows concentrations of olivine-rich materials. The color scale bar denotes a range of 0–100% concentrations in all images. Daytime band 9 radiance is used for shading in the images. (For interpretation of the references to color in this figure legend, the reader is referred to the web version of this article.)

tures are typically $10\text{--}20 \text{ cm}^{-1}$ lower (longer wavelengths) in the Gusev data. There is also a deeper broad absorption present at $\sim 1000\text{--}1100 \text{ cm}^{-1}$ in the Mini-TES data that is not as prominent in the TES data. This broad absorption is in the region of the main dust absorption however, and variation in the strength of this absorption is present between the individual Mini-TES rock spectra.

4. Discussion

4.1. Relationships at Gusev

The rock and dark soil compositions present in the Gusev Plains are relatively uniform and they bear spectral, mineralogical, and thermophysical similarities to units observed from orbit across larger regions. In this case, the high-thermal inertia surfaces are the rocks themselves, which also have elevated olivine contents and are similar in spectral signature and mineralogy to olivine-rich surfaces observed from orbit (Ruff et al., 2006; Fig. 13). Dark soils are similar in their spectral signature and mineralogy to equatorial low albedo surfaces and are missing the well-defined olivine spectral features present in the rock/high inertia surfaces. Although other mineralogical differences are likely present between the rocks and soils (sulfates and amorphous silica may also be present and variable; Yen et al., 2005; Ruff et al., 2006; Hamilton and Ruff, 2009), the difference in olivine content is the clearest and most prominent difference. This is supported by differences present in

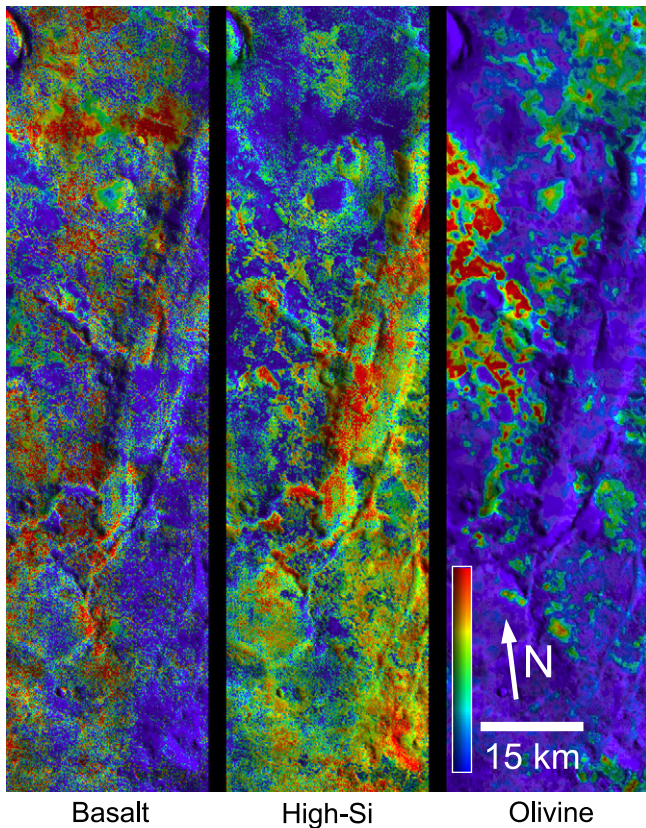


Fig. 6. Nili Fossae spectral endmember concentration maps for the region shown in Fig. 3 (THEMIS ID I02007009). The left image (basalt) shows concentrations of materials dominated by plagioclase and pyroxene, the center image (high-Si) shows concentrations of materials dominated by plagioclase and a high silica component, and the right image (olivine) shows concentrations of olivine-rich materials. The color scale bar denotes a range of 0–100% concentrations in all images. Daytime band 9 radiance is used for shading in the images. (For interpretation of the references to color in this figure legend, the reader is referred to the web version of this article.)

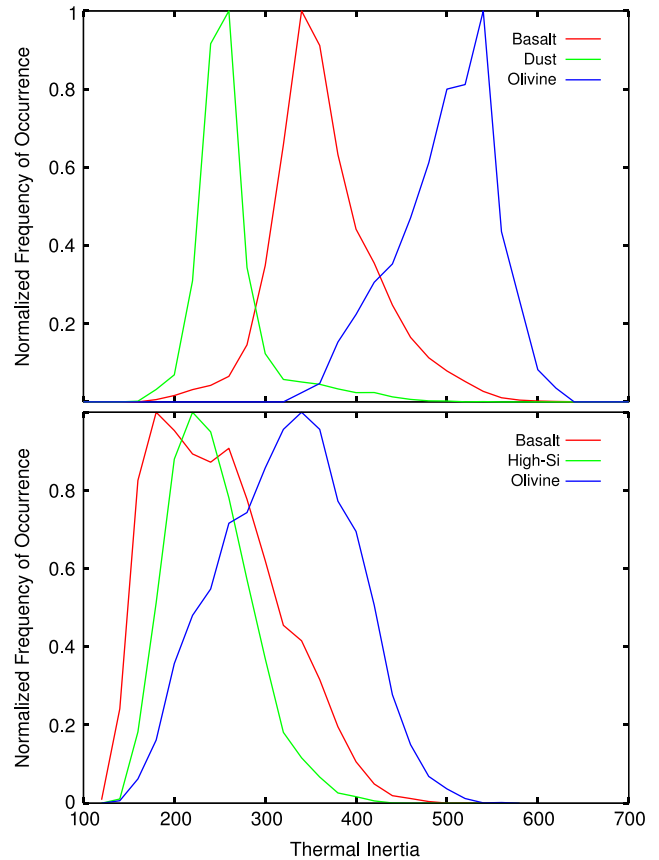


Fig. 7. Spectral endmember thermal inertia (units of $\text{J m}^{-2} \text{K}^{-1} \text{s}^{-1/2}$) histograms for Isidis Basin (top) and Nili Fossae (bottom). Data for each of the histograms were derived from pixels in the images shown in Figs. 5 and 6 with concentrations of >90% and with coverage overlapping with the thermal inertia data shown in Fig. 4.

Fe mineralogy indicated by Mössbauer spectrometer results (e.g. Morris et al., 2006).

The El Dorado sand spectra show a spectral shape that has olivine features that are clearly present, but are not as prominent as the Adirondack Class rocks. These sands are unusual in that they appear to be armored by particles that are distinctly larger (200–300 μm) than that of the dark soils and underlying sand (Sullivan et al., 2008). Sullivan et al., 2008 and Morris et al. (2008) also noted that the large particles have spectral features present in near-infrared and Mössbauer measurements consistent with an enhanced olivine content relative to the underlying finer materials (<100 μm) and Gusev Plains soils. In addition, Ming et al. (2008) note chemical similarities between the El Dorado sand and Adirondack Class rocks.

Although the processes responsible for the particle size distribution of the El Dorado sands are unclear, the trend of decreasing olivine content with decreasing particle size is the same as that of rocks and soils described here. The larger, less mechanically processed materials have more prominent olivine absorptions in Mini-TES spectra than finer particulate dark soils and less prominent absorptions when compared to Adirondack Class rocks. The El Dorado sands are located within the Columbia Hills with a large variety of lithologies and soil compositions and the source lithology of the sands remain unclear and may come from multiple sources (Ming et al., 2008). As a result, it is difficult to know the proper context of the compositional variations with respect to

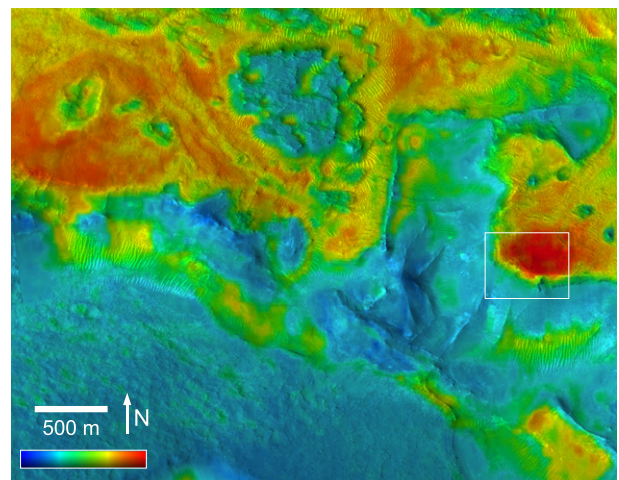


Fig. 8. CRISM olivine index (color scale; FRT00003E12_07) and HiRISE image (shading; PSP_002800_2025) of a portion of the image shown in Fig. 3 in Nili Fossae. More prominent olivine absorption features are associated with reds and oranges on the color scale, though olivine absorptions are present over all surfaces in the image. The white box denotes the area of detail shown in Fig. 10. (For interpretation of the references to color in this figure legend, the reader is referred to the web version of this article.)

the compositions within the more uniform Gusev Plains. However, it is a unique example of a clean material of intermediate particle

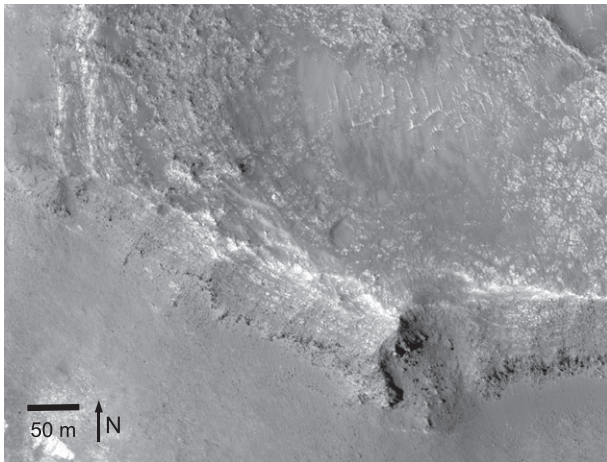


Fig. 9. HiRISE image (PSP_002800_2025) of a portion of the image shown in Fig. 8. More prominent olivine absorption features are associated with the relatively light-toned fractured terrain and the smooth featureless terrain on the top of the mesa. Relatively featureless materials located in the bottom and left portions of the image contain phyllosilicate as well as less prominent olivine absorption features as detailed by Mustard et al. (2009). Solar illumination is from the left.

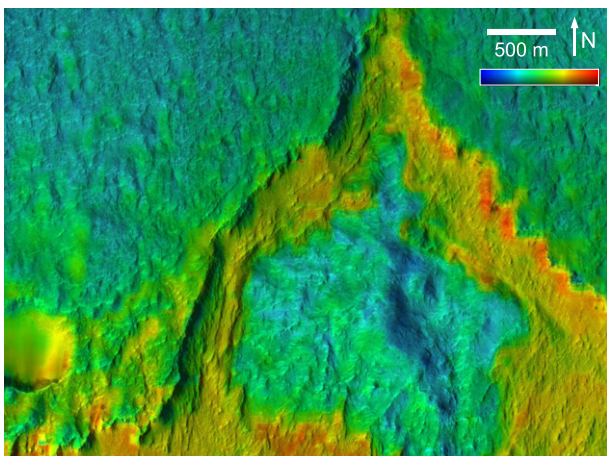


Fig. 10. CRISM olivine index (color scale; FRT00003E12_07) and HiRISE image (shading; PSP_002800_2025) of a portion of the image shown in Fig. 2 in the southern rim of Isidis Basin. More prominent olivine absorption features are associated with reds and oranges on the color scale. The layered resistant materials are associated with higher olivine concentrations. Although clear textural distinctions are not present at this scale, more prominent olivine absorptions are also associated with higher thermal inertia materials as can be seen in the detail of the nighttime temperature overlay image shown in Fig. 2. (For interpretation of the references to color in this figure legend, the reader is referred to the web version of this article.)

size and may represent an intermediate phase in the weathering of surface materials.

These large differences in olivine content are not obviously reflected in the elemental abundances derived from APXS measurements. Brushed Adirondack Class rock surfaces (no Mini-TES data of abraded rock surfaces are included because of interfering particle size effects) display a decrease of 1.4 wt.% in FeO content and a slight increase of 0.1 wt.% in MgO content relative to dark soils. Deconvolution results on Mini-TES and orbital TES datasets display a ~15–20% difference in olivine (areal) abundance (e.g. Hoefen et al., 2003; Rogers et al., 2005; Yen et al., 2005; Ruff et al., 2006).

APXS measurements show clear differences in sulfur content with highly correlated Cl abundances (e.g. Gellert et al., 2006). Assuming that S and Cl are the only external compositional inputs,

Table 1
Mini-TES observations used for this study.

| Sol | Target description | Observation ID |
|------------------------|--------------------|-----------------------------|
| <i>Rocks</i> | | |
| 14 | Adirondack | 2T127611250EDR0309P3110N0A1 |
| 41 | Gepetto | 2T130008664EDR0506P3149N0A1 |
| 41 | Sarah | 2T130008158EDR0506P3148N0A1 |
| 53 | Humphrey brushed | 2T131080845EDR1124P3166N0A1 |
| 100 | Route 66 brushed | 2T135242771EDR2702P3229N0A1 |
| <i>Dark soils</i> | | |
| 89 | Rover tracks | 2T134261556EDR2400P3660N0A1 |
| 93 | Rover tracks | 2T134627818EDR2700P3661N0A1 |
| 103 | Rover tracks | 2T135510179EDR2900P3664N0A1 |
| 105 | Rover tracks | 2T135685197EDR3000P3667N0A1 |
| 109 | Rover tracks | 2T136038679EDR3300P3668N0A1 |
| 122 | Rover tracks | 2T137195502EDR4204P3915N0A1 |
| 126 | Rover tracks | 2T137551700EDR4600P3916N0A1 |
| <i>El Dorado sands</i> | | |
| 709 | El Dorado surface | 2T189304161EDRAL00P3680N0A1 |
| 709 | El Dorado surface | 2T189298370EDRAL00P3680N0A1 |

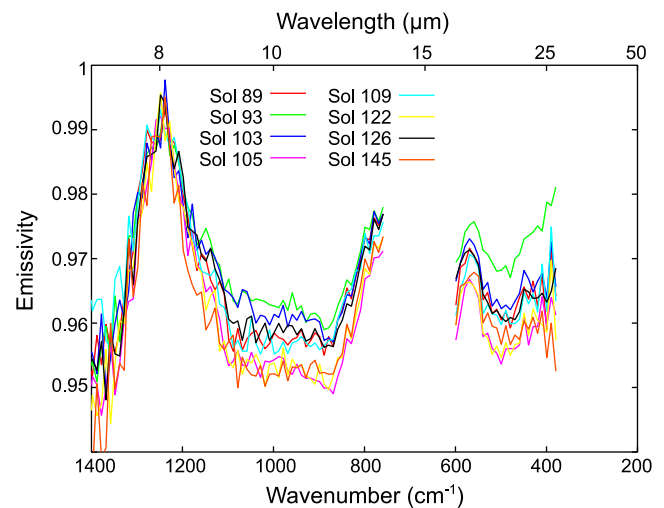


Fig. 11. Mini-TES emissivity spectra of dark soil surfaces within the Gusev Plains (listed in Table 1). All spectra cover rover tracks, which are free of thin high albedo dust coatings on the surface and are of sufficient temperatures to have high signal to noise ratios. The gap between ~600 and 750 cm^{-1} is due to atmospheric CO_2 .

the normalized abundances of major elemental compositions associated with mafic minerals (Mg, Ca, and Fe) show decreasing trends between the rocks, and soils and Si abundance increases. However, the relative abundances of the major cations analyzed on an AFK diagram (after that of Hurowitz et al. (2006) and Tosca et al. (2004)) do not show clear differences (Fig. 14). Although the absolute abundances of these elements are decreasing, they are decreasing in a roughly proportional manner. Under conditions involving significant aqueous alteration and transport, the relative proportions of these elements would be expected to show clear variations.

Alteration under martian surface conditions, which are presumably water-limited and likely to be acidic, is predicted to dissolve olivine at a much greater rate than other phases (e.g. Tosca et al., 2004; Hurowitz et al., 2006). This trend appears to be clearly reflected in the orbital and in situ mineralogical data, but not in the elemental data, which should show a decrease in Fe and Mg content relative to Al, Na, K, and Ca. Hurowitz et al. (2006) did note small but statistically significant chemical differences between brushed and RATted rocks within the Gusev Plains. These differences cannot be discriminated among the scatter of soil and rock

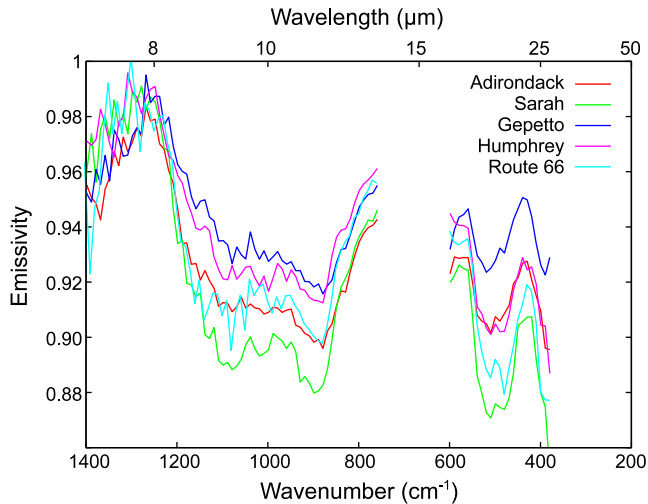


Fig. 12. Mini-TES emissivity spectra of Adirondack Class rocks within the Gusev Plains (listed in Table 1). All spectra cover either brushed or relatively dust-free surfaces and have sufficiently high temperatures to have high signal to noise ratios. No abraded rock surfaces are included because of the interfering effects of the resulting fine particulates. Spectra have been corrected using the methods of Ruff et al. (2006).

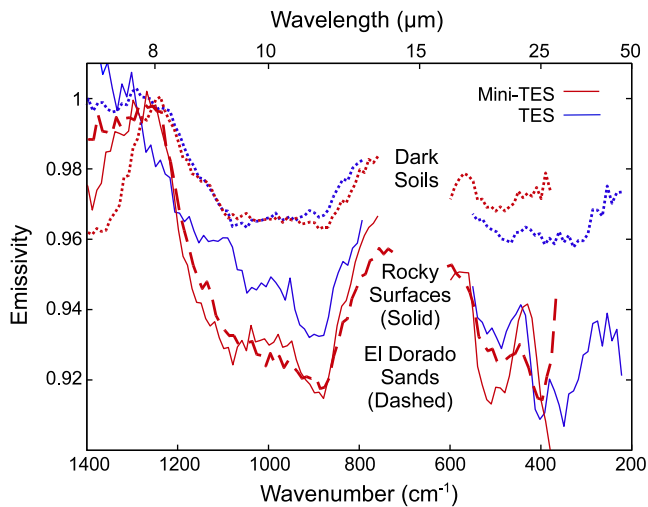


Fig. 13. Average Mini-TES emissivity spectra of Adirondack Class rocks (solid), El Dorado sands (medium dash), and Gusev Plains dark soils (fine dash) shown in Figs. 11 and 12 (red). TES surface emissivity spectra from equatorial dark regions (dark soils) and Nili Fossae (rocky surfaces) are shown for comparison (blue). Prominent olivine absorptions are present in the rocky surface spectra near 400, 500, and 875 cm^{-1} . The Nili Fossae and Gusev Plains rocky surfaces show slight differences in the precise wavelength of olivine absorptions, indicating slight differences in cation content (e.g. Koeppen and Hamilton, 2008). The El Dorado sand spectrum is of the relatively large particle size armored surface described by Sullivan et al. (2008) and has a spectral shape in-between that of the dark soils and rocks.

elemental measurements and are not of a sufficient magnitude to reflect the major changes in olivine content. Any alteration processes responsible for the formation of weathering rinds are likely similar to those involved in local soil formation.

It is difficult to identify a clear anchor point that relates the rocks and soils in the elemental abundance data because of the possible external inputs and alteration processes (e.g. Amundson et al., 2008). Gusev dark soils have a higher Si content (relative to other cations), but limited differences in the ratios of major cations to each other. In addition, relatively immobile minor element

abundances, such as Ti also show significant differences between rocks and soils (e.g. Yen et al., 2005). Indeed, a separate approach commonly used in terrestrial soil studies uses normalization of elemental abundances to Ti in order to track the relative losses of other elements due to weathering (Hausrath et al., 2008; Amundson et al., 2008).

4.2. Regional-global olivine and bedrock associations

There is a clear pattern of spatial correlation between olivine-rich surfaces and high-thermal inertia/rocky surfaces. This pattern extends to all scales from individual rocks and soils within the Gusev Plains to the global distributions. These correlations are clear, but not perfect, and any attempt to ascribe a single process or mechanism to the surface of an entire planet is likely to be oversimplified. Nevertheless, the strong association of olivine with high inertia materials strongly implies a causal relationship.

At the global scale, olivine-rich surfaces and very high-thermal inertia surfaces occur in similar regions including a restriction of occurrences to low- and mid-latitudes (Fig. 1). Edwards et al. (2009) found bedrock outcrops to be restricted to less than $\sim 45^\circ$ latitude corresponding to regions where periglacial processes appear to have broken down steep slopes and other potentially rocky surfaces (e.g. Kreslavsky et al., 2008). In addition, there are large low albedo regions at equatorial latitudes that do not have either high-thermal inertia surfaces or olivine-rich compositions, including Meridiani Planum and southern highlands surfaces southeast of Isidis Basin. The absence of olivine-rich and high-thermal inertia surfaces across extensive low albedo regions does not appear to be tied to a distinct property such as surface morphology or age. For example, there does not appear to be a common related property between Margaritifer Terra, Tyrrhena Terra, Hesperia Planum, and Meridiani Planum besides having a low albedo and being present at relatively low latitudes. This makes it difficult to attribute relatively simple properties such as age to the presence of olivine-rich and high-thermal inertia surfaces.

The correlation between high-thermal inertia and olivine-rich surfaces does appear to break down in some regions, such as the southern rim of Isidis Basin, which has extensive olivine-rich exposures but no extremely high inertia surfaces. However, as can be seen from the regional comparisons (Fig. 2), elevated thermal inertia surfaces are clearly present in the region and are indeed highly correlated with the olivine-rich surfaces. The definition of high-thermal inertia used by Edwards et al. (2009) was intended to define surfaces dominated by solid rock. This number ($1200 \text{ J m}^{-2} \text{ K}^{-1} \text{ s}^{-1/2}$) is higher than is required to define surfaces that are not composed of solid blocks/bedrock, but have not yet been mechanically processed into a sandy/silty soil. An additional example of this has been shown in Ares Valles, which does not have any high inertia exposures that satisfy the conditions of Edwards et al. (2009), but show clear correlations of high-thermal inertia surfaces with olivine-rich compositions (Rogers et al., 2005).

Despite these regional associations, the occurrence of very high-thermal inertia surfaces is not necessarily coincident with all olivine-rich compositions. The correlation is only regional, but not local in nature. It is clearly possible for rocky surfaces to be covered with a thin layer of dust and/or soil that could mask the compositional but not the thermophysical properties. Although this is almost certainly the case in some instances, to invoke dust coverage in every circumstance would be contrived. Indeed, many basaltic shergottites are clearly examples of unweathered olivine-poor rocks (though the mineralogy of martian meteorites are also a poor match for most martian surfaces; Hamilton et al., 2003).

The regional comparison of composition and thermal inertia in the southern rim of Isidis Basin and Nili Fossae show the correlation of these surfaces more precisely. The DCS mosaics show a

Table 2
APXS elemental abundances for abraded and brushed Adirondack Class rocks and dark soils within the Gusev Plains.

| Spectrum | Name | Na ₂ O (%) | MgO (%) | Al ₂ O ₃ (%) | SiO ₂ (%) | P ₂ O ₅ (%) | SO ₃ (%) | Cl (%) | K ₂ O (%) | CaO (%) | TiO ₂ (%) | Cr ₂ O ₃ (%) | MnO (%) | FeO (%) | Ni (ppm) | Zn (ppm) | Br (ppm) |
|------------------------|----------------------------|-----------------------|---------|------------------------------------|----------------------|-----------------------------------|---------------------|--------|----------------------|---------|----------------------|------------------------------------|---------|---------|----------|----------|----------|
| A034 | Adirondack RAT | 2.41 | 10.83 | 10.87 | 45.70 | 0.52 | 1.23 | 0.20 | 0.07 | 7.75 | 0.48 | 0.61 | 0.41 | 18.80 | 165 | 81 | 14 |
| A059_CS | Humphrey RAT1 | 2.76 | 9.49 | 10.78 | 46.30 | 0.57 | 1.09 | 0.32 | 0.13 | 8.19 | 0.58 | 0.68 | 0.41 | 18.60 | 202 | 117 | 49 |
| A060_CS | Humphrey RAT2 | 2.54 | 10.41 | 10.68 | 45.90 | 0.56 | 1.28 | 0.26 | 0.10 | 7.84 | 0.55 | 0.60 | 0.41 | 18.80 | 164 | 112 | 52 |
| A082_CS | Mazatzal | 2.74 | 9.02 | 9.92 | 45.70 | 0.82 | 3.33 | 0.54 | 0.29 | 7.57 | 0.69 | 0.45 | 0.40 | 18.40 | 342 | 222 | 144 |
| A086_CS | NewYork RAT1 | | | | | | | | | | | | | | | | |
| | Mazatzal | 2.78 | 9.72 | 10.70 | 45.80 | 0.65 | 1.48 | 0.23 | 0.16 | 8.02 | 0.59 | 0.54 | 0.42 | 18.90 | 132 | 75 | 161 |
| | Brooklyn RAT2 | | | | | | | | | | | | | | | | |
| Average abraded rock | | 2.65 | 9.89 | 10.59 | 45.88 | 0.62 | 1.68 | 0.31 | 0.15 | 7.87 | 0.58 | 0.58 | 0.41 | 18.70 | 201 | 121 | 84 |
| A033_S | Adirondack brush | 2.78 | 9.51 | 11.35 | 45.70 | 0.57 | 2.16 | 0.36 | 0.12 | 7.84 | 0.49 | 0.63 | 0.39 | 18.00 | 149 | 80 | 16 |
| A081A_CS | Mazatzal | 2.54 | 7.70 | 8.50 | 44.50 | 1.19 | 7.62 | 1.28 | 0.54 | 6.63 | 0.84 | 0.26 | 0.32 | 17.90 | 553 | 457 | 100 |
| | NewYork Brush | | | | | | | | | | | | | | | | |
| A100_CS | Route66 brushed | 2.88 | 8.67 | 10.78 | 44.80 | 0.74 | 4.20 | 0.55 | 0.23 | 7.83 | 0.59 | 0.53 | 0.39 | 17.70 | 181 | 125 | 46 |
| A058_CS | Humphrey brush | 2.95 | 8.82 | 11.20 | 45.90 | 0.62 | 2.63 | 0.49 | 0.18 | 7.76 | 0.54 | 0.60 | 0.39 | 17.90 | 158 | 95 | 37 |
| Average brushed rock | | 2.79 | 8.68 | 10.46 | 45.23 | 0.78 | 4.15 | 0.67 | 0.27 | 7.51 | 0.61 | 0.51 | 0.37 | 17.88 | 260 | 189 | 50 |
| A049_CS | Road Cut Floor3 | 2.44 | 8.90 | 9.83 | 46.20 | 0.68 | 6.11 | 0.69 | 0.38 | 6.14 | 1.00 | 0.43 | 0.34 | 16.80 | 443 | 318 | 61 |
| A050_CS | Road Cut | 2.65 | 8.77 | 9.96 | 46.10 | 0.73 | 5.69 | 0.77 | 0.37 | 6.24 | 1.02 | 0.40 | 0.35 | 16.80 | 592 | 255 | 65 |
| | WallMlonl | | | | | | | | | | | | | | | | |
| A113_CS | Bighole Mayfly surface | 3.10 | 8.39 | 9.92 | 46.10 | 0.88 | 6.37 | 0.79 | 0.47 | 6.07 | 1.00 | 0.37 | 0.31 | 16.10 | 467 | 192 | 32 |
| A114_CS | Bighole RS2 | 2.51 | 9.19 | 9.06 | 43.70 | 0.80 | 9.13 | 1.00 | 0.35 | 5.74 | 0.87 | 0.36 | 0.34 | 16.80 | 466 | 460 | 64 |
| A115_CS | Bighole Trico | 2.47 | 9.04 | 9.08 | 44.20 | 0.74 | 8.37 | 1.00 | 0.34 | 5.86 | 0.89 | 0.43 | 0.34 | 17.10 | 466 | 382 | 47 |
| A122_CS | Owens soil track | 3.07 | 8.41 | 10.65 | 47.00 | 0.95 | 5.45 | 0.63 | 0.47 | 6.38 | 0.88 | 0.33 | 0.28 | 15.40 | 391 | 239 | 31 |
| A135_CS | Santa Anita trench surface | 3.04 | 8.73 | 10.71 | 47.00 | 0.77 | 4.67 | 0.54 | 0.42 | 6.27 | 0.89 | 0.42 | 0.34 | 16.10 | 483 | 291 | 19 |
| Average dark soil | | 2.75 | 8.78 | 9.89 | 45.76 | 0.79 | 6.54 | 0.77 | 0.40 | 6.10 | 0.94 | 0.39 | 0.33 | 16.44 | 473 | 305 | 46 |
| A709_CS | ElDorado Scuff Shadow | 3.01 | 11.31 | 10.74 | 46.90 | 0.81 | 3.06 | 0.38 | 0.31 | 6.10 | 0.62 | 0.32 | 0.31 | 16.00 | 997 | 114 | 22 |
| A710_CS | ElDorado Scuff Edgar | 3.17 | 10.04 | 10.93 | 47.50 | 0.75 | 3.26 | 0.42 | 0.37 | 6.28 | 0.73 | 0.34 | 0.31 | 15.80 | 684 | 145 | 29 |
| Average El Dorado sand | | 3.09 | 10.68 | 10.84 | 47.20 | 0.78 | 3.16 | 0.40 | 0.34 | 6.19 | 0.68 | 0.33 | 0.31 | 15.90 | 841 | 130 | 26 |

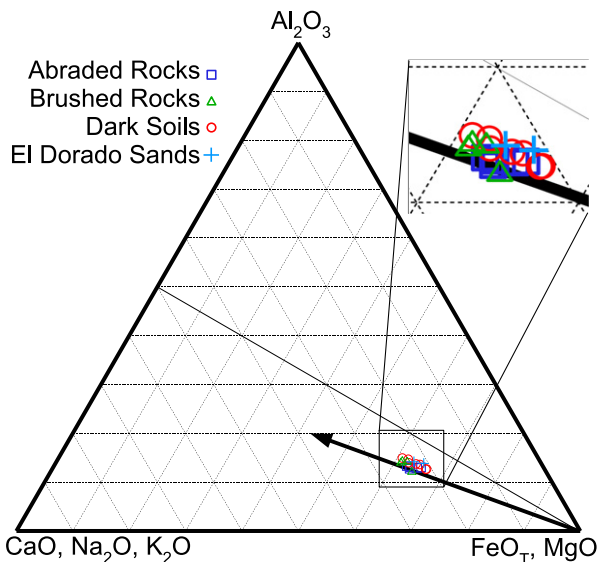


Fig. 14. APXS derived oxides plotted in molar abundance (after Hurwitz et al. (2006)). All samples were acquired in the Gusev Plains and individual observations are listed in Table 1. All rocks are Adirondack Class compositions and dark soils are from rover tracks or dark soils within trenches. The arrow denotes the predicted compositional trend under water-limited acidic weathering conditions.

prevalence of purple and magenta colors that are largely spatially coincident with elevated nighttime temperatures (Figs. 2 and 3). This is not without exception, however, as relatively cold nighttime

Table 3
Average APXS derived oxide abundances normalized for SO₃ and Cl content.

| | Na ₂ O (%) | MgO (%) | Al ₂ O ₃ (%) | SiO ₂ (%) | CaO (%) | FeO (%) |
|----------------------|-----------------------|---------|------------------------------------|----------------------|---------|---------|
| Average abraded rock | 2.7 | 10.1 | 10.8 | 46.9 | 8.0 | 19.1 |
| Average brushed rock | 2.9 | 9.1 | 11.0 | 47.6 | 7.9 | 18.8 |
| Average dark soil | 3.0 | 9.5 | 10.7 | 49.4 | 6.6 | 17.8 |
| Average El Dorado | 3.2 | 11.1 | 11.2 | 49.0 | 6.4 | 16.5 |

temperatures (and presumably low thermal inertia) are coincident with olivine-rich surfaces in several areas within Nili Fossae (typically lavender in color in the DCS mosaic shown in Fig. 3). This can also be seen in the surface composition/thermal inertia histograms (Fig. 7) for Nili Fossae that shows a lower thermal inertia tail present in its distribution for olivine-rich surfaces. This indicates that materials can be broken down mechanically via a process that preserves the olivine. Conversely, high inertia surfaces that are olivine-poor are present in the northeast portion of Fig. 3. This has been noted by Hamilton and Christensen (2005) and is presumably due to a thin covering of dust, which is responsible for the higher albedo of the region.

Although the correlation appears to be stronger in the southern rim of Isidis Basin, both regions show an association of olivine-rich surfaces with elevated thermal inertia values of ~300–600 (Figs. 4–7). This is much lower than the thermal inertia value of 1200 used to define rocky units and is more consistent with gravel assuming a uniform particle size (Presley and Christensen, 1997). It is signifi-

cantly greater than the values of ~ 150 – 300 typical of martian low albedo regions and consistent with martian sandy/silty soils (e.g. Ferguson et al., 2006b). Although the interpretation of these values of thermal inertia are non-unique, the olivine-rich surfaces rarely have thermophysical properties consistent with sandy/silty soils.

These observations are supported by high-resolution imagery. The olivine-rich surfaces are associated with surfaces that are either layered, heavily fractured, or contain local concentrations of rocks (Figs. 8–10). This is consistent with the higher thermal inertia values and the presence of materials that have experienced less mechanical processing than typical martian dark soils. Textures at high resolution are not always correlated with olivine content, however. For example, Figs. 8 and 9 show smooth, relatively featureless terrain in Nili Fossae that contains prominent olivine absorptions in CRISM data. Fig. 10 shows some association of olivine-rich surfaces with layered materials, but other surfaces may or may not have elevated olivine contents without a clear distinguishing texture. However, in both cases, olivine-rich surfaces are associated with high-thermal inertia values and nearby low thermal inertia surfaces do not have elevated olivine contents. This indicates that different surface physical properties are present despite textural similarities at the sub-meter scale of HiRISE images. Although it is possible that dust cover in some areas of Isidis Planitia may obscure the spectral identification of olivine-rich surfaces, the areas shown in the case of Nili Fossae are dust-free and still contain large amounts of basaltic materials.

Tornabene et al. (2008) and Mustard et al. (2009) documented some of these thermophysical and textural relationships. In both the southern rim of Isidis Basin and Nili Fossae the olivine-rich unit is overlain by a mafic unit composed primarily of plagioclase and pyroxene with a relatively low olivine content. Tornabene et al. (2008) noted a similar difference in thermophysical properties of olivine-rich and olivine-poor surfaces as shown here. Tornabene et al. (2008) suggested that the difference in thermophysical properties indicates a difference in post-emplacment processing of the thermophysical/compositional units rather than simply a difference in lava composition.

4.3. Synthesis of observations

These geochemical and mineralogical relationships are consistent with chemical alteration in an acidic water-limited environment. Chemical trends between rock surfaces and interiors have been shown to be consistent with this type of weathering environment (e.g. Hurowitz et al., 2006). Under these conditions, olivine would be much more rapidly weathered than other materials such as plagioclase and pyroxene. Although the elemental trends between rock interiors, surfaces, and soils are subtle and potentially complex, Mini-TES and Mössbauer observations show distinct trends in olivine abundance that confirm the elemental trend between rock interiors and surfaces and extend this trend to sands and soils. Olivine abundances decrease from rock interiors, rock surfaces, coarse sands, to fine sand/silty soils. As on Earth, mechanical and chemical weathering appear to be strongly associated with each other at Gusev Crater.

The examples shown here in Nili Fossae and Isidis Planitia show the same relationship between olivine and particle size. This is in addition to similar examples that have been noted in Argyre Planitia (Bandfield and Rogers, 2008), Ares Valles (Rogers et al., 2005), and Valles Marineris (Edwards et al., 2008). This trend extends globally; regions that have high olivine abundances are coincident with regions that have high-thermal inertia units.

It is possible that sands, soils, and rocks are unrelated and originate from separate sources. However, that scenario presents several difficulties; (1) as discussed above, the major cation ratios of soils are coincidentally nearly identical to that of the rocks even

though major differences are present in mineralogy and (2) there is no identified source of unweathered materials besides the Adirondack Class rocks in the region.

Limited water may be available to dissolve minerals on the martian surface, but not transport any elements a significant distance before re-precipitation. It is likely that this could occur in-place, such on the local rock surface. In this manner, fractionation of species of variable solubility is prevented from occurring and yet large changes in mineralogy are expected. This “cation conservative” weathering has been suggested to occur on Mars in other situations (e.g. Niles and Michalski, 2008).

The dissolution of olivine is expected to result in the locally precipitated amorphous silica and oxides. The reduction in olivine content is clear in both Mini-TES and Mössbauer data. The presence of amorphous silica phases is ambiguous and they are more difficult to detect than changes in the magnitude of narrow and prominent olivine absorptions. However, high-silica phases are commonly present in regional soils and are not detected in olivine-rich surfaces using orbital data (Hoefen et al., 2003; Rogers and Christensen, 2007). Although not detected in the Mini-TES data, there are also clear differences in oxides present between rock and soils indicated by the Mössbauer data (Morris et al., 2006).

This does not account for all of the observations, however. Other inputs must be present to explain the differences in abundances of elements, such as Ti, S, K, Ni, and Si. Yen et al. (2006) show that differences in Ni contents are consistent with a meteoric component to the soils. Differences in K contents imply either a different source composition or significant alteration. It is also difficult to understand the differences in Ti content without the presence of an external source of material. It is clear that soil formation on Mars, even within the limited area of the Gusev Plains, is influenced by multiple processes. For example, it is possible that aeolian fractionation of higher density Fe and Ti oxide minerals may be responsible for these compositional differences (McLennan, 2000; McSween and Keil, 2000).

Despite this complexity, we still consider the observations most consistent with limited aqueous alteration under conditions similar to those of the current martian climate. The implication is that most martian surfaces have experienced some degree of aqueous alteration and that liquid water has played a larger role in surface processes than has been previously recognized. The geochemical relationships are bolstered by spatial relationships that indicate olivine-rich source and olivine-poor sediment materials, such as in Argyre Planitia (Bandfield and Rogers, 2008).

The global observations are consistent with the local observations within the Gusev Plains but the stratigraphic relationships between olivine-rich and olivine-poor compositions are complicated (e.g. Rogers et al., 2008). It is not possible to invoke an earlier (or later) period of more intense weathering as the sole explanation for olivine-poor materials. Indeed the olivine-rich composition in Nili Fossae is sandwiched in-between phyllosilicate bearing materials and olivine-poor materials (Mustard et al., 2009). High-thermal inertia, olivine-rich surfaces are commonly found within layers of limited stratigraphic extent (e.g. Edwards et al., 2008). If these surfaces simply represent lava flows of a different composition from the typical upper martian crust, it would be required that olivine-poor compositions exposed on the martian surface consist largely of low thermal inertia, easily eroded volcanic ash or some other poorly consolidated unweathered material. Under this scenario, explosive volcanism would be dominated by olivine-poor compositions and solid lava flows/sills are dominated by olivine-rich compositions.

Although this is not necessarily our favored hypothesis, this relationship appears to be a possibility, especially because large

volumes of pyroclastic materials have been proposed to be present on the martian surface (e.g. Wilson and Head, 2007). If martian dark soils consist largely of unweathered basaltic ash or related deposits, the upper martian crust may be dominated by poorly coherent materials that are relatively easy to break down. This would also explain the relative lack of high-thermal inertia materials present on steep surfaces such as canyon and crater walls.

If high-thermal inertia surfaces are unique in representing relatively unaltered materials, it may indicate that martian igneous compositions are dominated by mafic, olivine-rich compositions. McSween et al. (2006) noted this possible relationship and surmised that primitive, olivine-rich basalts may be more representative of the martian surface than previously recognized based on remote sensing datasets. It may be more difficult than previously assumed to clearly identify and locate examples of unaltered compositions on the martian surface.

4.4. Implications for remote sensing

Regardless of the formation mechanism involved, the combination of measurements acquired at the Gusev Plains provides a useful example of how the datasets should be interpreted. For example, the APXS measurements show elevated sulfur contents on rock surfaces and dark soils that are assumed to be present as sulfates (e.g. Clark, 1981). Although sulfates are retrieved from deconvolution analysis of TIR data near the detection limits within many low albedo regions, including at Gusev (Yen et al., 2005; Rogers and Christensen, 2007; Rogers and Aharonson, 2008), they have not been identified with a high degree of confidence. Near-infrared spectroscopy has not detected the presence of sulfates in these low albedo regions as well. Amorphous silica is often detected in the TIR data, but its provenance is ambiguous. However, amorphous silica is a predicted weathering product in the martian environment (e.g. McLennan, 2003; Tosca et al., 2004; Hurowitz et al., 2006, 2007; McSween et al., 2006) along with iron oxides (which are not expected to be detected; e.g. Minitti et al., 2007). The presence of amorphous silica is common throughout martian low albedo regions (Rogers and Christensen, 2007), including in the Gusev dark soils (Yen et al., 2005) and is consistent with formation via chemical weathering.

Conversely, APXS results have been used to show alteration trends, but these trends are not nearly as apparent as is shown by mineralogical differences between surfaces. In this case, olivine is easily distinguished spectrally from amorphous silica and oxide materials, but if the dissolution and re-precipitation occurs locally, elemental measurements will not distinguish between weathered and unweathered materials.

We have taken somewhat for granted that the lack of evidence for alteration products makes it safe to assume that surface materials consist of primary compositions. However, the link between remotely sensed data and primary igneous compositions is not so direct, especially with soils (McSween et al., 2006; Bandfield and Rogers, 2008). This adds a further layer of complexity to the analysis of the data, but also allows for a more robust characterization of the processes that have influenced the martian surface.

If large regions of Mars have been altered, there are implications for previous studies that have linked remote sensing measurements to martian meteorite compositions (e.g. Mustard et al., 1997; Hamilton et al., 2003). Surface Types 1 and 2 (Bandfield et al., 2000) do not match known martian meteorite compositions and only isolated locations match the bulk mineralogy of certain meteorites such as ALH84001 (Hamilton et al., 2003). However, the conclusion that martian meteorites are not typical (near surface) martian igneous materials may not be as valid if surface materials are overwhelmingly dominated by broken down and altered materials. In any case, if Adirondack Class basalts are typical

martian igneous compositions, then martian meteorites are still not a good mineralogical match and it remains necessary to bury or hide the source of the meteorites within dusty regions such as Tharsis.

The work presented here has focused on olivine-rich materials or compositions similar to the Surface Type 1 of Bandfield et al. (2000). Although this surface type may be generalized as a single spectral unit, Rogers and Christensen (2007) have shown that regional variations are present in plagioclase, pyroxene, and olivine abundances. These variations are consistent with pyroxene compositional variations identified in NIR data (e.g. Bibring et al., 2005) and this may reflect variations in the original unaltered composition.

Surface Type 2 materials, which are dominated by plagioclase and amorphous silica remain ambiguous in origin (e.g. Kraft et al., 2003; Ruff and Christensen, 2007). The amorphous silica-rich phase can be interpreted as sedimentary silica or primary volcanic glass. There seems to be clear evidence for both types of silica-rich phases on Mars (e.g. Christensen et al., 2005; Bandfield, 2008; Milliken et al., 2008). However, among the large regions covered by Surface Type 2 materials, there are currently no measurements that show similar geochemical and morphological relationships to those shown here. Because we have not observed high inertia units adjacent to Surface Type 2 materials at high or low latitudes, it is not possible to test the spatial and mineralogical associations in a manner similar to what has been presented here.

Nonetheless, it does seem likely that if Surface Type 1 has been significantly altered, Surface Type 2 has been altered as well. The nature of the source material for Surface Type 2 is perhaps even less well understood, but the amorphous Si-rich component has been proposed as a product of aqueous alteration under similar water-limited and/or low pH conditions as the mechanisms described here for Surface Type 1 materials (e.g. Kraft et al., 2003; Minitti et al., 2007).

5. Conclusions

Previous work has shown that olivine dissolution via acidic weathering may explain subtle chemical trends observed between rock rinds and interiors on the Gusev Plains (Hurowitz et al., 2006). Mineralogical trends obtained from rocks and soils within the Gusev Plains are much more prominent and indicate that olivine weathering has likely occurred. This suggests that chemical weathering is closely linked with physical weathering and soil formation. However, clear differences are also present in elemental abundances that indicate a variety of inputs and processes are likely responsible for the formation of martian dark soils. As an alternative, it is possible that the relatively olivine-poor soils represent a largely unaltered and separate primary source lithology.

The correlation between olivine abundance and particle size is also observed at regional and global scales. There is a strong spatial correlation between olivine-rich and high-thermal inertia surfaces at global, regional, and local scales on Mars. Though not without exception, sandy/silty soils on Mars are typically olivine-poor relative to adjacent rocks or rocky surfaces even where the rocky materials are the likely source for the sediments. The trends indicate that martian soils have likely been altered to some degree during the process of separation from the source rock. However, because regional differences are present in the primary mineralogy (Rogers et al., 2007), original igneous compositional variations also appear to be present though the source of these materials may be consistently more mafic than previously recognized.

It is important to understand the limitations of interpreting null results in the individual datasets. Martian equatorial dark regions have often been considered unaltered based on the lack of second-

ary minerals detected from spectroscopic measurements. Elemental abundances do not show differences in composition in the Gusev Plains as clearly as measurements that are sensitive to mineralogy, such as those acquired by Mössbauer, and Mini-TES.

Despite the potential complexity of source materials and processes, it appears that most martian dark regions have likely experienced aqueous alteration. The influence of water on the martian surface may be more extensive than previously realized and chemical weathering appears to be closely linked to the mechanical breakdown of materials. Despite the near-ubiquitous presence of soils on the martian surface, processes involved in soil formation on Mars remain largely unknown. Measurements and observations that trace the properties from the source materials to the soils can be used to better understand martian climate and the integrated effects of water related processes throughout its history.

Acknowledgments

We would like to thank Phil Christensen and Vicky Hamilton in particular for numerous lively discussions. Thanks also to Ronald Amundson, Tim Glotch, Joel Hurowitz, Amy Knudson, Mike Kraft, Hap McSween, Paul Niles, Steve Ruff, Brad Sutter, and Nick Tosca for attempting to clarify our questions and ideas. Two anonymous reviewers provided useful and constructive comments and suggestions that significantly improved this manuscript. This work was partially funded by grants from the Mars Data Analysis Program awarded to JLB (NNX08AK52G) and ADR (NNX08AL10G).

References

- Amundson, R., Ewing, S., Dietrich, W., Sutter, B., Owen, J., Chadwick, O., Nishiizumi, K., Walvoord, M., McKay, C., 2008. On the in situ aqueous alteration of soils on Mars. *Geochim. Cosmochim. Acta*. doi:10.1016/j.gca.2008.04.038.
- Bandfield, J.L., 2008. High-silica deposits of an aqueous origin in western Hellas Basin, Mars. *Geophys. Res. Lett.* 35. doi:10.1029/2008GL033807.
- Bandfield, J.L., Edwards, C.S., 2008. Derivation of martian surface slope characteristics from directional thermal infrared radiometry. *Icarus* 193, 139–157.
- Bandfield, J.L., Feldman, W.C., 2008. Martian high latitude permafrost depth and surface cover thermal inertia distributions. *J. Geophys. Res.* 113. doi:10.1029/2007JE003007.
- Bandfield, J.L., Rogers, A.D., 2008. Olivine dissolution by acidic fluids in Argyre Planitia, Mars: Evidence for a widespread process? *Geology*. doi:10.1130/G24724A.1.
- Bandfield, J.L., Smith, M.D., 2003. Multiple emission angle surface–atmosphere separations of Thermal Emission Spectrometer data. *Icarus* 161, 47–65.
- Bandfield, J.L., Hamilton, V.E., Christensen, P.R., 2000. A global view of martian surface compositions from MGS-TES. *Science* 287, 1626–1630. doi:10.1126/science.287.5458.1626.
- Bandfield, J.L., Rogers, A.D., Smith, M.D., Christensen, P.R., 2004a. Atmospheric correction and surface spectral unit mapping using Thermal Emission Imaging System data. *J. Geophys. Res.* 109. doi:10.1029/2004JE002289.
- Bibring, J.-P. et al., 2005. Mars Surface Diversity as Revealed by the OMEGA/Mars Express Observations. *Science* 307. doi:10.1126/science.1108806.
- Bandfield, J.L., Rogers, D., Smith, M.D., Christensen, P.R., 2004b. Atmospheric correction and surface spectral unit mapping using Thermal Emission Imaging System data. *J. Geophys. Res.* 109. doi:10.1029/2004JE002289.
- Buczowski, D.L., Murchie, S.L., Seelos, F.P., Malaret, E., Hash, C., and Crism Team, 2008. CRISM analyses of Argyre Basin. *Lunar Planet. Sci.* XXXIX, 39 (Abstract 1391).
- Christensen, P.R. et al., 2003. Miniature Thermal Emission Spectrometer for the Mars Exploration Rovers. *J. Geophys. Res.* 108. doi:10.1029/2003JE002117.
- Christensen, P.R., Jakosky, B.M., Kieffer, H.H., Malin, M.C., McSween Jr., H.Y., Nealon, K., Mehall, G.L., Silverman, S.H., Ferry, S., Caplinger, M., et al., 2004. The Thermal Emission Imaging System (THEMIS) for the Mars 2001 Odyssey Mission. *Space Sci. Rev.* 110, 85–130.
- Christensen, P.R. et al., 2005. Evidence for magmatic evolution and diversity on Mars from infrared observations. *Nature* 436, 504–509.
- Clark, B.C., Van Hart, D.C., 1981. The salts of Mars. *Icarus* 45, 370–378.
- Edwards, C.S., Christensen, P.R., Hamilton, V.E., 2008. Evidence for extensive olivine-rich basalt bedrock outcrops in Ganges and Eos chasmas, Mars. *J. Geophys. Res.* 113. doi:10.1029/2008JE003091.
- Edwards, C.S., Bandfield, J.L., Christensen, P.R., Fergason, R.L., 2009. Global distribution of bedrock exposures on Mars using THEMIS high-resolution thermal inertia. *J. Geophys. Res.* 114. doi:10.1029/2009JE003363.
- Fergason, R.L., Christensen, P.R., Kieffer, H.H., 2006a. High-resolution thermal inertia derived from the Thermal Emission Imaging System (THEMIS): Thermal model and applications. *J. Geophys. Res.* 111. doi:10.1029/2006JE002735.
- Fergason, R.L., Christensen, P.R., Bell III, J.F., Golombek, M.P., Herkenhoff, K.E., Kieffer, H.H., 2006b. Physical properties of the Mars Exploration Rover landing sites as inferred from Mini-TES derived thermal inertia. *J. Geophys. Res.* 111. doi:10.1029/2005JE002583.
- Gellert, R. et al., 2006. Alpha particle X-ray spectrometer (APXS): Results from Gusev Crater and calibration report. *J. Geophys. Res.* doi:10.1029/2005JE002555.
- Gendrin, A. et al., 2005. Sulfates in martian layered terrains: The OMEGA/Mars Express view. *Science* 307, 1587–1591.
- Gillespie, A.R., Kahle, A.B., Walker, R.E., 1986. Color enhancement of highly correlated images: I. Decorrelation and HIS contrast stretches. *Remote Sens. Environ.* 20, 209–235.
- Glotch, T.D., Bandfield, J.L., Christensen, P.R., Calvin, W.M., McLennan, S.M., Clark, B.C., Rogers, A.D., Squyres, S.W., 2006. Mineralogy of the light-toned outcrop at Meridiani Planum as seen by the Miniature Thermal Emission Spectrometer and implications for its formation. *J. Geophys. Res.* 111. doi:10.1029/2005JE002672.
- Hamilton, V.E., Christensen, P.R., 2000. Determining the modal mineralogy of mafic and ultramafic igneous rocks using thermal emission spectroscopy. *J. Geophys. Res.* 105, 9717–9733.
- Hamilton, V.E., Christensen, P.R., 2005. Evidence for extensive, olivine-rich bedrock on Mars. *Geology* 33, 433–436.
- Hamilton, V.E., Ruff, S.W., 2009. Mini-TES spectra of Mazatzal and other Adirondack-Class basalts in Gusev Crater, Mars: Spectral/mineralogical evidence for alteration. *Lunar Planet. Sci.* 40 (Abstract 1418).
- Hamilton, V.E., Christensen, P.R., McSween Jr., H.Y., Bandfield, J.L., 2003. Searching for the source regions of martian meteorites using MGS TES: Integrating martian meteorites into the global distribution of volcanic materials on Mars. *Meteorit. Planet. Sci.* 38, 871–886.
- Hausrath, E.M., Navarre-Sitchler, A.K., Sak, P.B., Steefel, C.I., Brantley, S.L., 2008. Basalt weathering rates on Earth and the duration of liquid water on the plains of Gusev Crater, Mars. *Geology*. doi:10.1130/G24238A.1.
- Hoefen, T.M., Clark, R.N., Bandfield, J.L., Smith, M.D., Pearl, J.C., Christensen, P.R., 2003. Discovery of olivine in the Nili Fossae region of Mars. *Science* 302. doi:10.1126/science.1089647.
- Hurowitz, J.A., McLennan, S.M., 2007. A ~3.5 Ga record of water-limited, acidic weathering conditions on Mars. *Earth Planet. Sci. Lett.* 260. doi:10.1016/j.epsl.2007.05.043.
- Hurowitz, J.A., McLennan, S.M., Tosca, N.J., Arvidson, R.E., Michalski, J.R., Ming, D.W., Schröder, C., Squyres, S.W., 2006. In situ and experimental evidence for acidic weathering of rocks and soils on Mars. *J. Geophys. Res.* 111. doi:10.1029/2005JE002515.
- Jenny, H., 1941. *Factors of Soil Formation: A Quantitative Pedology*. McGraw-Hill, New York.
- Keller, J.M., Boynton, W.V., Karunatillake, S., Baker, V.R., Dohm, J.M., Evans, L.G., Finch, M.J., Hahn, B.C., Hamara, D.K., Janes, D.M., et al., 2006. Equatorial and midlatitude distribution of chlorine measured by Mars Odyssey GRS. *J. Geophys. Res.* doi:10.1029/2006JE002679.
- Kieffer, H.H., Martin, T.Z., Peterfreund, A.R., Jakosky, B.M., Miner, E.D., Palluconi, F.D., 1977. Thermal and albedo mapping of Mars during the viking primary mission. *J. Geophys. Res.* 82, 4249–4291.
- Kieffer, H.H., Christensen, P.R., Titus, T.N., 2006. CO₂ jets formed by sublimation beneath translucent slab ice in Mars' seasonal south polar ice cap. *Nature* 442. doi:10.1038/nature04945.
- Koepfen, W.C., Hamilton, V.E., 2008. Global distribution, composition, and abundance of olivine on the surface of Mars from thermal infrared data. *J. Geophys. Res.* 113. doi:10.1029/2007JE002984.
- Kraft, M.D., Michalski, J.R., Sharp, T.G., 2003. Effects of pure silica coatings on thermal emission spectra of basaltic rocks: Considerations for martian surface mineralogy. *Geophys. Res. Lett.* 30. doi:10.1029/2003GL018848.
- Kreslavsky, M.A., Head, J.W., Marchant, D.R., 2008. Periods of active permafrost layer formation during the geological history of Mars: Implications for circum-polar and mid-latitude surface processes. *Planet. Space. Sci.* 56. doi:10.1016/j.pss.2006.02.010.
- McEwen, A.S. et al., 2007. Mars Reconnaissance Orbiter's High Resolution Imaging Science Experiment (HiRISE). *J. Geophys. Res.* 112. doi:10.1029/2005JE002605.
- McGuire, P.C. et al., 2009. An improvement to the volcano-scan algorithm for atmospheric correction of CRISM and OMEGA spectral data. *Planet. Space. Sci.* 57. doi:10.1016/j.pss.2009.03.007.
- McLennan, S.M., 2000. Chemical composition of martian soil and rocks: Complex mixing and sedimentary transport. *Geophys. Res. Lett.* 27, 1335–1338.
- McLennan, S.M., 2003. Sedimentary silica on Mars. *Geology* 31, 315–318.
- McSween Jr., H.Y., Keil, K., 2000. Mixing relationships in the martian regolith and the composition of globally homogeneous dust. *Geochim. Cosmochim. Acta* 64, 2155–2166.
- McSween, H.Y. et al., 2006. Characterization and petrologic interpretation of olivine-rich basalts at Gusev Crater, Mars. *J. Geophys. Res.* 111. doi:10.1029/2005JE002477.
- Milliken, R.E., Swayze, G.A., Arvidson, R.E., Bishop, J.L., Clark, R.N., Ehmann, B.L., Green, R.O., Grotzinger, J.P., Morris, R.V., Murchie, S.L., et al., 2008. Opaline silica in young deposits on Mars. *Geology* 36. doi:10.1130/G24967A.1.
- Ming, D.W. et al., 2008. Geochemical properties of rocks and soils in Gusev Crater, Mars: Results of the Alpha Particle X-Ray Spectrometer from Cumberland Ridge to Home Plate. *J. Geophys. Res.* 113. doi:10.1029/2008JE003195.

- Minitti, M.E., Weitz, C.M., Lane, M.D., Bishop, J.L., 2007. Morphology, chemistry, and spectral properties of Hawaiian rock coatings and implications for Mars. *J. Geophys. Res.* 112. doi:10.1029/2006JE002839.
- Morris, R.V. et al., 2006. Mössbauer mineralogy of rock, soil, and dust at Gusev crater, Mars: Spirit's journey through weakly altered olivine basalt on the plains and pervasively altered basalt in the Columbia Hills. *J. Geophys. Res.* 111. doi:10.1029/2005JE002584.
- Morris, R.V. et al., 2008. Iron mineralogy and aqueous alteration from Husband Hill through Home Plate at Gusev Crater, Mars: Results from the Mössbauer instrument on the Spirit Mars Exploration Rover. *J. Geophys. Res.* 113. doi:10.1029/2008JE003201.
- Murchie, S. et al., 2007. CRISM multispectral summary products: Parameterizing mineral diversity on Mars from reflectance. *J. Geophys. Res.* 112. doi:10.1029/2006JE002831.
- Mustard, J.F., Murchie, S., Erard, S., Sunshine, J., 1997. In situ compositions of martian volcanics: Implications for the mantle. *J. Geophys. Res.* 102, 25605–25616.
- Mustard, J.F., Poulet, F., Gendrin, A., Bibring, J.-P., Langevin, Y., Gondet, B., Mangold, N., Bellucci, G., Altieri, F., 2005. Olivine and pyroxene diversity in the crust of Mars. *Science* 307, 1594–1597.
- Mustard, J.F., Ehlmann, B.L., Murchie, S.L., Poulet, F., Mangold, N., Head, J.W., Bibring, J.P., Roach, L.H., 2009. Composition, morphology, and stratigraphy of Noachian crust around the Isidis Basin. *J. Geophys. Res.* doi:10.1029/2009JE003349.
- Niles, P.B., Michalski, J., 2008. Meridiani Planum sediments on Mars formed through weathering in massive ice deposits. *Nat. Geosci.* 2. doi:10.1038/ngeo438.
- Pelkey, S.M. et al., 2007. CRISM multispectral summary products: Parameterizing mineral diversity on Mars from reflectance. *J. Geophys. Res.* 112. doi:10.1029/2006JE002831.
- Poulet, F., Bibring, J.-P., Mustard, J.F., Gendrin, A., Mangold, N., Langevin, Y., Arvidson, R.E., Gondet, B., Gomez, C., 2005. Phyllosilicates on Mars and implications for early martian climate. *Nature*. doi:10.1038/nature04274.
- Presley, M., Christensen, P., 1997. The effect of bulk density and particle size sorting on the thermal conductivity of particulate materials under martian atmospheric pressures. *J. Geophys. Res.* 102, 9221–9229.
- Ramsey, M.S., Christensen, P.R., 1998. Mineral abundance determination: Quantitative deconvolution of thermal emission spectra. *J. Geophys. Res.* 103, 577–596.
- Rieder, R., Gellert, R., Brückner, J., Klingelhöfer, G., Dreibus, G., Yen, A., Squyres, S.W., 2003. The new Athena alpha particle X-ray spectrometer for the Mars Exploration Rovers. *J. Geophys. Res.* 108. doi:10.1029/2003JE002150.
- Rogers, A.D., Aharonson, O., 2008. Mineralogical composition of sands in Meridiani Planum determined from Mars Exploration Rover data and comparison to orbital measurements. *J. Geophys. Res.* 113. doi:10.1029/2007JE002995.
- Rogers, A.D., Bandfield, J.L., 2009. Mineralogical characterization of Mars Science Laboratory candidate landing sites from THEMIS and TES data. *Icarus*. doi:10.1016/j.icarus.2009.04.020.
- Rogers, A.D., Christensen, P.R., 2007. Surface mineralogy of martian low-albedo regions from MGS-TES data: Implications for upper crustal evolution and surface alteration. *J. Geophys. Res.* 112. doi:10.1029/2006JE002727.
- Rogers, A.D., Christensen, P.R., Bandfield, J.L., 2005. Compositional heterogeneity of the ancient martian crust: Analysis of Ares Vallis bedrock with THEMIS and TES data. *J. Geophys. Res.* 110. doi:10.1029/2005JE002399.
- Rogers, A.D., Bandfield, J.L., Christensen, P.R., 2007. Global spectral classification of martian low-albedo regions with Mars Global Surveyor Thermal Emission Spectrometer (MGS-TES) data. *J. Geophys. Res.* 112. doi:10.1029/2006JE002726.
- Rogers, A.D., Aharonson, O., Bandfield, J.L., 2009. Geologic context of in situ rocky exposures in Mare Serpentis, Mars: Implications for crust and regolith evolution in the cratered highlands. *Icarus* 200. doi:10.1016/j.icarus.2008.11.026.
- Ruff, S.W., Christensen, P.R., 2007. Basaltic andesite, altered basalt, and a TES-based search for smectite clay minerals on Mars. *Geophys. Res. Lett.* 34. doi:10.1029/2007GL029602.
- Ruff, S.W., Christensen, P.R., Blaney, D.L., Farrand, W.H., Johnson, J.R., Michalski, J.R., Moersch, J.E., Wright, S.P., Squyres, S.W., 2006. The rocks of Gusev Crater as viewed by the Mini-TES instrument. *J. Geophys. Res.* 111. doi:10.1029/2006JE002747.
- Schneider, R.D., Hamilton, V.E., 2006. Evidence for locally derived, ultramafic intracrater materials in Amazonis Planitia, Mars. *J. Geophys. Res.* 111. doi:10.1029/2005JE002611.
- Smith, M.D., Bandfield, J.L., Christensen, P.R., 2000. Separation of surface and atmospheric spectral features in Mars Global Surveyor Thermal Emission Spectrometer (TES) spectra. *J. Geophys. Res.* 105, 9589–9608.
- Sullivan, R. et al., 2008. Wind-driven particle mobility on Mars: Insights from Mars Exploration Rover observations at 'El Dorado' and surroundings at Gusev Crater. *J. Geophys. Res.* 113. doi:10.1029/2008JE003101.
- Thomson, J.L., Salisbury, J.W., 1993. The mid-infrared reflectance of mineral mixtures (7–14 μm). *Remote Sens. Environ.* 43, 1–13.
- Titus, T.N., Kieffer, H.H., Christensen, P.R., 2003. Exposed water ice discovered near the south pole of Mars. *Science* 299, 1048–1051.
- Tornabene, L.L., Moersch, J.E., McSween Jr., H.Y., Hamilton, V.E., Piatek, J.L., Christensen, P.R., 2008. Surface and crater-exposed lithologic units of the Isidis Basin as mapped by coanalysis of THEMIS and TES derived data products. *J. Geophys. Res.* 113. doi:10.1029/2007JE002988.
- Tosca, N.J., McLennan, S.M., Lindsley, D.H., Schoonen, M.A.A., 2004. Acid-sulfate weathering of synthetic martian basalt: The acid fog model revisited. *J. Geophys. Res.* 109. doi:10.1029/2003JE002218.
- Wilson, L., Head, J.W., 2007. Explosive volcanic eruptions on Mars: Tephra and accretionary lapilli formation, dispersal and recognition in the geologic record. *J. Volc. Geotherm. Res.* 163. doi:10.1016/j.jvolgeores.2007.03.007.
- Yen, A.S. et al., 2005. An integrated view of the chemistry and mineralogy of martian soils. *Nature* 436. doi:10.1038/nature03637.
- Yen, A.S. et al., 2006. Nickel on Mars: Constraints on meteoritic material at the surface. *J. Geophys. Res.* 111. doi:10.1029/2006JE002797.